NEUROSCIENCE

Tripartite extended amygdala–basal ganglia CRH circuit drives locomotor activation and avoidance behavior

Simon Chang[1], Federica Fermani[2], Chu-Lan Lao[3], Lianyun Huang[4], Mira Jakovcevski[1]†, Rossella Di Giaimo[5,6], Miriam Gagliardi[7], Danusa Menegaz[8], Alexandru Adrian Hennrich[9], Michael Ziller[7], Matthias Eder[8], Rüdiger Klein[2], Na Cai[4], Jan M. Deussing[1]*

An adaptive stress response involves various mediators and circuits orchestrating a complex interplay of physiological, emotional, and behavioral adjustments. We identified a population of corticotropin-releasing hormone (CRH) neurons in the lateral part of the interstitial nucleus of the anterior commissure (IPACL), a subdivision of the extended amygdala, which exclusively innervate the substantia nigra (SN). Specific stimulation of this circuit elicits hyperactivation of the hypothalamic-pituitary-adrenal axis, locomotor activation, and avoidance behavior contingent on CRH receptor type 1 (CRHR1) located at axon terminals in the SN, which originate from external globus pallidus (GPe) neurons. The neuronal activity prompting the observed behavior is shaped by IPACL^{CRH} and GPe^{CRHR1} neurons coalescing in the SN. These results delineate a previously unidentified tripartite CRH circuit functionally connecting extended amygdala and basal ganglia nuclei to drive locomotor activation and avoidance behavior.

INTRODUCTION

Striving for homeostasis, the body reacts to real or perceived stressors through coordinated activation of various effector systems and brain circuits (*1*). Severe or chronic stress combined with a maladaptive stress response is well-known risk factors for neuropsychiatric disorders, such as anxiety, depression, and addiction (*2*, *3*). Corticotropin-releasing hormone (CRH), a central mediator of the stress response (*4*), is released in response to salient environmental stimuli activating the neuroendocrine stress axis (*5*) and promoting arousal (*6*–*8*), as well as anxiety- and fear-related behaviors (*9*–*14*). This evolutionary conserved peptide is expressed throughout the central nervous system. Depending on its localization, it has been implicated in various aspects of the stress response (*15*). The response is intrinsically tied to physiological arousal, which is essential for fast adaptation including decisions on whether to approach or avoid a threat (*16*). Central application or overexpression of CRH has been demonstrated to induce arousal, locomotor, and behavioral activation paralleling a physiological stress response (*6*–*8*, *17*–*19*).

In recent years, the edging of mouse genetic tools and viral vectors including valid CRH system–related Cre drivers (*20*, *21*) has notably advanced our understanding of CRH neuron distribution, identity, connectivity, and function in the mouse brain (*13*, *20*, *22*–*24*). CRH circuits have been shown to play an important role in shaping the activity of various neurotransmitter and modulatory systems (*9*, *11*, *25*). Along these lines, we and others have demonstrated the connectivity and functional cross-talk of CRH neurons in the bed nucleus of the stria terminalis (BNST), central amygdala (CeA), and nucleus accumbens with dopaminergic circuits of the ventral tegmental area (VTA) thereby linking the stress response to dopamine (DA) regulation (*9*, *13*, *26*–*28*). CRH modulates the release of DA, producing a positive affective state (*9*, *13*, *29*). However, severe stress is able to abolish CRH's capacity to regulate DA release and to switch the CRH effect from appetitive to aversive (*27*). Midbrain DA neurons of the VTA and substantia nigra (SN) are part of the basal ganglia circuitry. While the VTA is classically implicated in behaviors related to reward and motivation controlled via mesolimibic/mesocortical pathways, the SN is related to movement initiation and coordination via the nigrostriatal pathway. Both aspects of basal ganglia function contribute to an adaptive response to stressful events (*30*–*33*). Similar to the VTA, the SN also expresses high levels of the CRH receptor type 1 (CRHR1) in not only dopaminergic but also GABAergic [γ-aminobutyric acid (GABA)–releasing] neurons, while local sources of CRH are largely absent from the SN (*9*). The direct role of the CRH system and thereby governed circuits modulating SN activity and its potential effect on locomotor function are not yet understood.

In this study, we identified a previously for the most part overlooked population of CRH neurons in the lateral division of the interstitial nucleus of the posterior limb of the anterior commissure (IPACL), which exclusively innervates the SN. Chemogenetic and optogenetic stimulation revealed that these CRH neurons promote locomotor and behavioral activation. Moreover, concomitant hyperreactivity of the neuroendocrine stress response and initiation of avoidance behavior suggest that specific CRH neuron stimulation is perceived as aversive. Last, we demonstrated that those behavioral effects are conveyed via presynaptic CRHR1 localized to axon terminals in the SN that have their origin in the external globus pallidus (GPe). Our study provides first evidence that the CRH system is functionally linked to basal ganglia circuits predominantly involved in movement initiation and coordination.

[1]Molecular Neurogenetics, Max Planck Institute of Psychiatry, Munich, Germany. [2]Molecules-Signaling-Development, Max Planck Institute for Biological Intelligence (in foundation), Martinsried, Germany. [3]Collaborative Research Centre/Sonderforschungsbereich (SFB) 870, Viral Vector Facility, Munich, Germany. [4]Translational Genetics, Helmholtz Pioneer Campus, Helmholtz Zentrum München, Munich, Germany. [5]Developmental Neurobiology, Max Planck Institute of Psychiatry, Munich, Germany. [6]Department of Biology, University of Naples Federico II, Naples Italy. [7]Genomics of Complex Diseases, Max Planck Institute of Psychiatry, Munich, Germany. [8]Scientific Core Unit Electrophysiology, Max Planck Institute of Psychiatry, Munich, Germany. [9]Max von Pettenkofer-Institute Virology, Medical Faculty, and Gene Center, Ludwig Maximilians University Munich, Munich, Germany.
*Corresponding author. Email: deussing@psych.mpg.de
†Present address: Functional Epigenetics in the Animal Model, Institute for Biology II, RWTH Aachen University, Aachen, Germany.

RESULTS

CRH neurons are enriched in the IPACL

We used the well-established CRH-Cre::Ai9 reporter mouse line (*13*, *20*) to assess the brain-wide distribution of CRH neurons. Imaging of cleared brains revealed an ensemble of CRH neurons at the transition between the CeA and BNST defined as IPAC, a structure previously assigned to the extended amygdala (*34*). In particular, the IPACL contains tdTomato$^+$ neurons in numbers comparable to the CeA and BNST (Fig. 1, A and B, and movies S1 and S2). Double in situ hybridization (ISH) confirmed that 95% of tdTomato$^+$ cells coexpress *Crh* mRNA validating the reporter as a reliable proxy for CRH neurons in the IPACL (Fig. 1C). Notably, the CAG promotor used in the Ai9 reporter line is not active in all *Crh* mRNA–expressing neurons of the IPACL. Intersectional CRH-Cre::Vgat-FlpO::Ai65 reporter mice revealed that IPACL^{CRH} neurons are GABAergic (Fig. 1D). Moreover, these neurons are characterized by their expression of wolframin endoplasmic reticulum transmembrane glycoprotein 1 (WFS1; 61 ± 8.5%) or calbindin (CALB; 35.1 ± 8.5%) with 15.0 ± 1.4% of neurons showing coexpression of both markers. A minor fraction is also positive for somatostatin (SOM; 1.7 ± 0.3%), whereas IPACL^{CRH} neurons do not express other markers of GABAergic neuronal subpopulations such as parvalbumin (PV), calretinin, or protein kinase Cδ (Fig. 1E and fig. S1, A to F).

Further characterization of IPACL neurons by whole-cell patch-clamp recordings revealed that CRH$^+$ and CRH$^-$ neurons display strong inward rectification, a depolarizing ramp potential, regular firing characteristics, and a remarkably low resting membrane potential (<−80 mV) (Fig. 1, F to H), all of which is typical for GABAergic spiny projection neurons (*35*, *36*). In addition, CRH$^+$ neurons have higher input resistance and lower rheobase, indicating a higher excitability compared to CRH$^-$ neurons (Fig. 1H). IPACL^{CRH} neurons receive glutamatergic and GABAergic synaptic inputs (Fig. 1I).

Stimulation of IPACL^{CRH} neurons triggers locomotor activation and avoidance behavior

To interrogate the function of this previously unexplored population of CRH$^+$ neurons, we used Cre-dependent adeno-associated viruses (AAVs) to express hM3Dq in IPACL^{CRH} neurons of CRH-Cre mice (Fig. 2A and fig. S2A), which were activated upon Clozapine-N-oxide (CNO) treatment as indicated by enhanced cFOS expression (Fig. 2B). As a mediator of the stress response, CRH serves as a secretagogue-triggering hypothalamic-pituitary-adrenal (HPA) axis activity and as a neuromodulator, it is implicated in the expression of stress-related behaviors. Activation of IPACL^{CRH} neurons in hM3Dq-expressing mice resulted in hyperactivation of the HPA axis compared to control mice as indicated by increased plasma corticosterone levels 30 and 90 min after CNO administration (Fig. 2C). To determine the temporal kinetics of behavioral responses to CNO-induced IPACL^{CRH} neuron activation, mice were subjected to a 90-min open-field test (OF). Mice expressing hM3Dq showed significantly elevated locomotor activity compared to control mice, peaking 15 min after CNO administration (fig. S2B). On the basis of this observation, we conducted different behavioral tasks assessing locomotor activity, exploratory, and anxiety-related behavior. CNO-treated mice expressing hM3Dq showed hyperactivity and delayed habituation in the OF and the dark light box (DaLi) (Fig. 2, D and E). C57BL/6N mice treated with CNO did not show any behavioral alterations in the OF or DaLi ruling out unspecific effects of the treatment (fig. S2, D and E). Together with the increased response of the HPA axis, these behavioral results suggest that stimulation of IPACL^{CRH} neurons is perceived as aversive triggering locomotor activation and potentially avoidance behavior. To further substantiate this hypothesis, we additionally conducted a conditioned place preference paradigm (CPP). hM3Dq-expressing mice showed clear avoidance of the CNO-paired chamber, while no difference in preference was observed in control animals (Fig. 2, F and G), thus corroborating the notion that the stimulation of IPACL^{CRH} neurons is perceived as an aversive stimulus that entails locomotor activation and avoidance behavior.

IPACL^{CRH} neurons specifically innervate the SN

To comprehend the efferent projections of IPACL^{CRH} neurons, we injected a Cre-dependent AAV into extended amygdala nuclei of CRH-Cre::Ai9 reporter mice to express the presynaptic marker synaptophysin–green fluorescent protein (Syn-GFP) in CRH$^+$ neurons (fig. S3, A to E). Within the extended amygdala, IPACL^{CRH} neurons presented a distinct pattern of distant projections (fig. S3, C and E, and movie S3). The preeminent accumulation of CRH terminals readily observable in the SN of CRH-Cre::Ai9 animals is apparently composed to a large extent of IPACL^{CRH} neuron terminals (Fig. 3, A and B, and movie S4). These terminals have a high CRH content as detected by immunohistochemistry (Fig. 3C). Injection of AAV-CreOFF/FlpON–enhanced yellow fluorescent protein (EYFP) into the IPACL of CRH-Cre::Vgat-FlpO::Ai65 mice revealed that efferents of GABAergic IPACL CRH$^-$ neurons were detectable throughout the SN and VTA (Fig. 3D), whereas terminals of IPACL^{CRH} neurons were specifically confined to the SN (Fig. 3E). Next, we injected the retrograde tracer FluoroGold (FG) into the SN of CRH-Cre::Ai9 reporter mice (Fig. 3F). Retrogradely labeled cells were detected in all brain regions previously shown to innervate the SN (*37*). In addition and in line with anterograde viral tracing, we observed a substantial number of FG-labeled CRH neurons in the CeA and IPACL (Fig. 3, G and H).

Stimulation of IPACL^{CRH} neuron efferents in the SN conveys avoidance behavior

The specificity and prominence of projections of IPACL^{CRH} neurons raised the intriguing question of whether these are sufficient to convey the observed behavioral response following stimulation of IPACL^{CRH} neurons. To address this, we first established whether optogenetic activation of IPACL^{CRH} neurons can mimic the effects of their chemogenetic activation. Therefore, we subjected mice selectively expressing ChR2 in IPACL^{CRH} neurons (Fig. 4A and fig. S4A) to a real-time place preference test (RTPP). Illumination of Channelrhodopsin-2 (ChR2)–expressing neurons directly in the IPACL resulted in neuronal activation (Fig. 4B and fig. S4B) and significant avoidance of the light-paired chamber (Fig. 4, C and D) recapitulating the consequences of CNO-induced activation of IPACL^{CRH} neurons during the conditioning phase. Next, we performed the RTPP but exclusively illuminated terminals of IPACL^{CRH} neurons in the SN resulting in enhanced cFOS expression in the IPACL (Fig. 4, E and F). Similar to the direct IPACL stimulation, ChR2-expressing mice also responded with strong place avoidance compared to control mice (Fig. 4, G and H). These findings indicate that the IPACL-SN projection is sufficient to drive the observed locomotor activation and avoidance behavior. The direct impact of IPACL^{CRH} neurons on the SN is further supported by the observation that the CNO-induced activation of IPACL^{CRH} neurons entailed enhanced cFOS expression in the SN (fig. S2C).

As chemogenetic and optogenetic activation approaches may drive nonphysiological responses, we assessed the consequences of IPACL^{CRH}

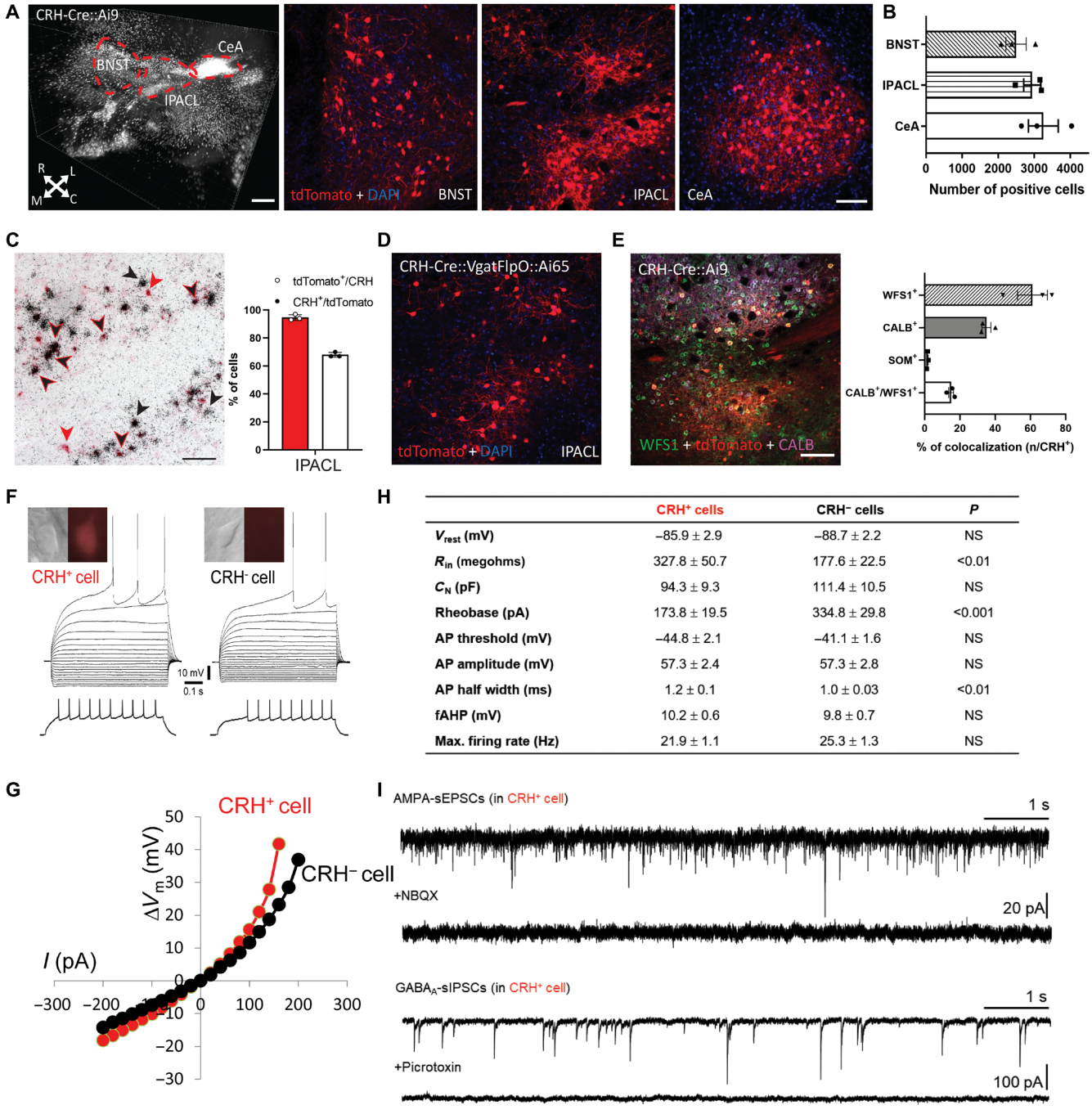

	CRH⁺ cells	CRH⁻ cells	*P*
V_{rest} (mV)	−85.9 ± 2.9	−88.7 ± 2.2	NS
R_{in} (megohms)	327.8 ± 50.7	177.6 ± 22.5	<0.01
C_N (pF)	94.3 ± 9.3	111.4 ± 10.5	NS
Rheobase (pA)	173.8 ± 19.5	334.8 ± 29.8	<0.001
AP threshold (mV)	−44.8 ± 2.1	−41.1 ± 1.6	NS
AP amplitude (mV)	57.3 ± 2.4	57.3 ± 2.8	NS
AP half width (ms)	1.2 ± 0.1	1.0 ± 0.03	<0.01
fAHP (mV)	10.2 ± 0.6	9.8 ± 0.7	NS
Max. firing rate (Hz)	21.9 ± 1.1	25.3 ± 1.3	NS

Fig. 1. Identification and characterization of IPACL^{CRH} neurons. (**A**) Snapshot of a cleared CRH-Cre::Ai9 brain showing tdTomato/CRH-expressing neurons throughout the extended amygdala and representative images depicting tdTomato-expressing CRH$^+$ neurons in subdivisions of the extended amygdala. Scale bars, 500 μm. DAPI, 4′,6-diamidino-2-phenylindole. (**B**) Quantification of CRH neurons in the CeA, IPACL, and BNST. (**C**) Specificity of Cre recombinase expression was confirmed by double ISH against tdTomato (red) and endogenous CRH mRNA expression (black silver grains). Scale bar, 200 μm. Quantification of tdTomato$^+$ neurons coexpressing CRH and CRH$^+$ neurons coexpressing tdTomato. Representative tdTomato$^+$ (red arrowheads), CRH$^+$ (black arrowheads) and coexpressing cells (black arrowheads with red contour) are indicated ($n = 3$ mice, 5 sections per mouse). (**D**) Tdtomato-expressing neurons in CRH-Cre::Vgat-FlpO::Ai65 intersectional reporter mice demonstrate that IPACL^{CRH} neurons are GABAergic. (**E**) Representative images from CRH-Cre::Ai9 mice depicting IPACL^{CRH} neurons costained with markers of GABAergic neurons WFS1, CALB, and SOM and quantification of colocalization. Scale bar, 200 μm (D and E). (**F**) Whole-cell patch-clamp recordings. (**G**) Current-voltage relationship. (**H**) Basic intrinsic properties of IPACL neurons (CRH$^+$, $n = 15/5$ mice; CRH$^-$, $n = 16/4$ mice). V_{rest}, resting membrane potential; R_{in}, input resistance; C_N, cell capacitance; AP, action potential; fAHP, fast after hyperpolarization; NS, not significant. Values represent means ± SEM. Two-tailed unpaired *t* test was used for statistical analysis. (**I**) Upper representative recording traces show spontaneous AMPA receptor–mediated excitatory postsynaptic currents (AMPA-sEPSCs) in a CRH$^+$ cell, which were completely blocked by NBQX (2,3-dihydroxy-6-nitro-7-sulfamoylbenzo[*f*]quinoxaline6-nitro-7-sulfamoylbenzo[*f*]quinoxaline-2,3-dione). Lower traces demonstrate spontaneous GABA$_A$ receptor–mediated inhibitory postsynaptic currents (GABA$_A$-sIPSCs) in a CRH$^+$ neuron that totally disappeared in the presence of picrotoxin.

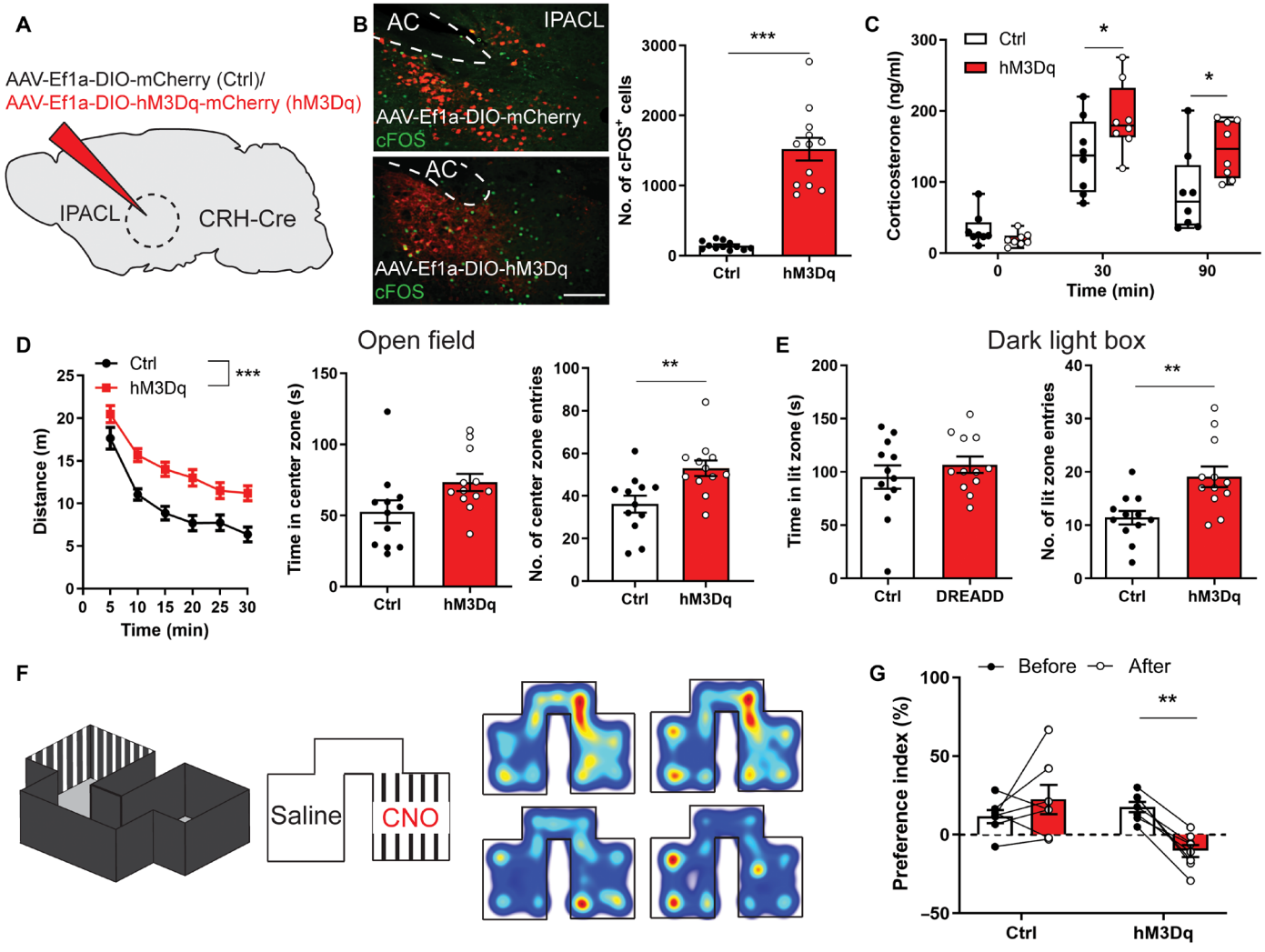

Fig. 2. Neuroendocrine and behavioral consequences of IPACL^{CRH} neuron activation. (**A**) Scheme illustrating injection of control (AAV$_8$-hSyn-DIO-mCherry) and hM3Dq-expressing (AAV$_8$-hSyn-DIO-hM3Dq-mCherry) virus into the IPACL. (**B**) Representative images of coronal IPACL sections and quantification of cFOS-positive cells. Scale bar, 200 μm. (**C**) Plasma corticosterone levels at baseline, 30 and 90 min following CNO administration [$n = 8$ per group; repeated-measures two-way analysis of variance (ANOVA), $F_{2,42} = 42.7$, $P < 0.0001$; Bonferroni's multiple comparison test, 30 min, $P = 0.047$; 90 min, $P = 0.03$]. (**D** to **G**) CNO treatment induces locomotor activation, delayed habituation, and avoidance behavior in hM3Dq-expressing animals. (D) Distance traveled ($n = 12$ per group; repeated-measures two-way ANOVA, $F_{1,22} = 17.49$, $P = 0.0004$), time spent in center ($P = 0.5$, $t = 2.1$), and transitions into the center zone ($P = 0.005$, $t = 3.1$) of the OF. (E) Time spent in lit zone ($n = 12$ per group; $P = 0.4$, $t = 0.85$) and entries into lit zone ($P = 0.003$, $t = 3.3$) of the DaLi. (F) Schematic illustration of place preference paradigm. Heat maps illustrating the accumulated time animals stayed in respective chambers before and after conditioning. (G) Calculated preference index ($n = 7$ per group; two-way ANOVA, Bonferroni's multiple comparison test, $P = 0.006$, $t = 3.70$). Values represent means ± SEM, *$P < 0.05$, **$P < 0.01$, and ***$P < 0.0001$.

neuron inhibition. To this end, we expressed halorhodopsin in IPACL^{CRH} neurons by injecting AAV-Ef1a-DIO-eNpHR3.0 into CRH-Cre mice (Fig. 4I). In the RTPP, inhibition of IPACL^{CRH} neurons resulted in preference of the light-paired chamber of mice expressing eNpHR3.0, while control animals did not show any preference (Fig. 4, J and K). Optogenetic inhibition of IPACL^{CRH} neurons did not significantly affect locomotor activation in the OF and in the DaLi. Only the time spent in the lit zone was increased (fig. S5, A to F).

Behavioral consequences of IPACL^{CRH} neuron activation are CRHR1 dependent

To understand whether the behavioral consequences of IPACL^{CRH} neuron activation can be directly attributed to CRH release and downstream activation of CRH receptors, we repeated the behavioral paradigms while blocking the high-affinity CRHR1 using the specific small-molecule antagonist R121919 (Fig. 5A). Systemic treatment of hM3Dq-expressing mice with R121919 was sufficient to attenuate the CNO-induced increase in cFOS expression in the SN (Fig. 5B) and blocked the CNO-induced increase in locomotor activity and entries to the center zone in the OF (Fig. 5C). In the DaLi, CRHR1 antagonism reduced the CNO-induced increase in transitions into the lit zone without affecting the time spent in that compartment compared to mice treated with CNO only (Fig. 5D). To rule out unspecific behavioral effects of the CRHR1 antagonist, we compared C57BL/6N mice treated with R121919 versus saline-treated animals. We did not observe any significant differences in the OF and DaLi (fig. S2, D and E). In the

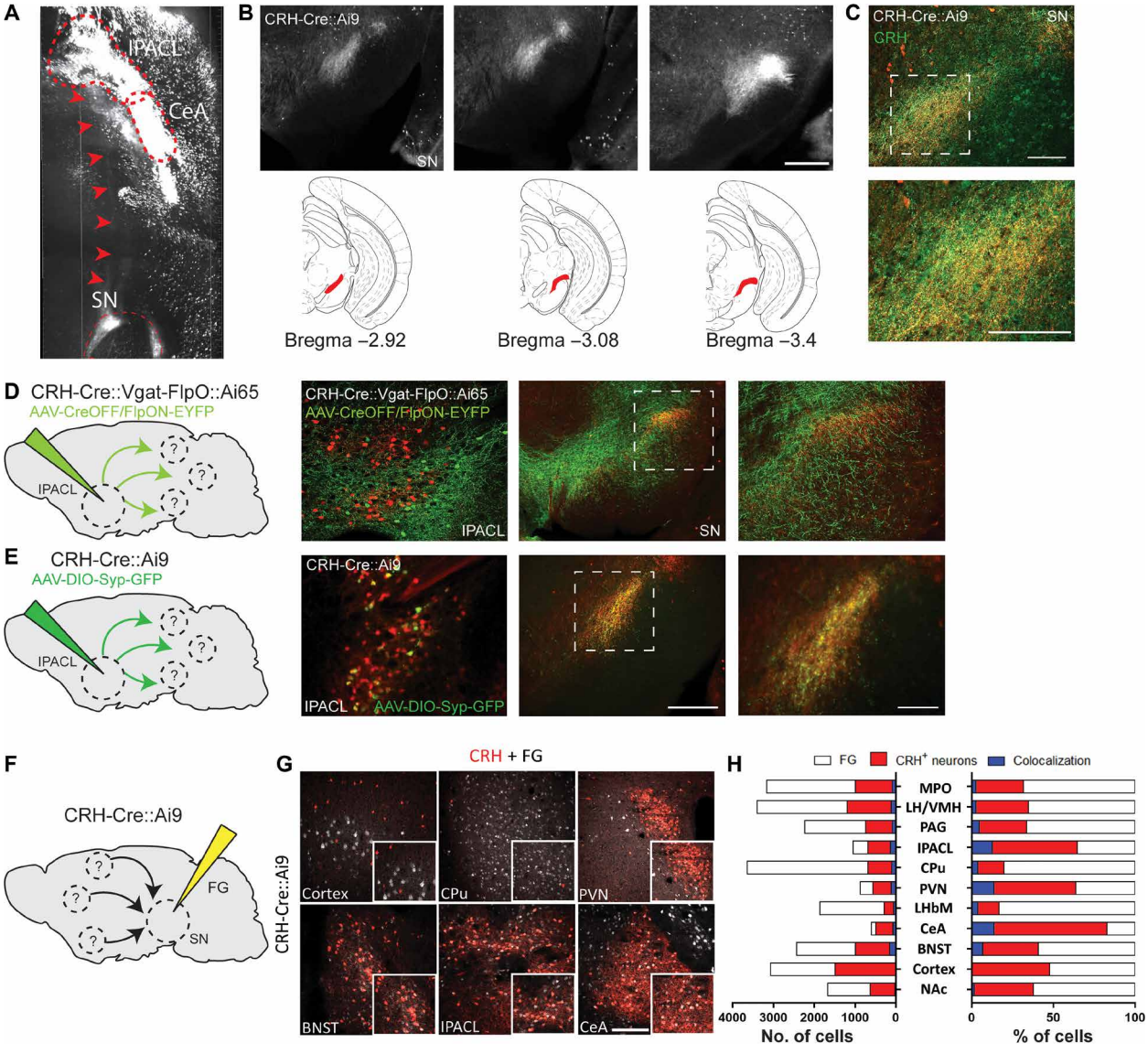

Fig. 3. Anterograde and retrograde tracing of IPACL^{CRH} neurons. (**A**) Representative horizontal section of a cleared CRH-Cre::Ai9 brain showing projections (arrowheads) from the IPACL to the SN. (**B**) Coronal vibratome sections of a CRH-Cre::Ai9 brain reveal accumulation of CRH neuron terminals in the SN. (**C**) Representative images of coronal brain sections of CRH-Cre::Ai9 mice showing axon terminals in the SN stained for CRH. (**D**) Scheme illustrating injection of AAV$_{DJ}$-hSyn-CreOff/FlpOn-EYFP into IPACL of CRH-Cre::Vgat-FlpO::Ai65 mice. Representative image of the injection site (left) and target area in the SN (middle). Higher magnification of marked area is shown to the left. (**E**) Scheme illustrating injection of AAV$_9$-CMV-DIO-Syp-GFP into IPACL of CRH-Cre::Ai9 mice. Representative images of the injection site (left) and respective target area in the SN (middle) with higher magnification of marked area shown to the left. (**F**) Scheme illustrating injection of FG into the SN of CRH-Cre::Ai9 animals. (**G**) Representative images of various brain regions demonstrating localization of FG in tdTomato-expressing CRH neurons. (**H**) Quantification of FG labelled CRH neurons throughout the brain following injection into the SN of CRH-Cre::Ai9 mice.

CPP, R121919 treatment prevented the place avoidance caused by the CNO-induced activation of IPACL^{CRH} neurons during conditioning (Fig. 5, E and F). Together, our data indicate that activation of IPACL^{CRH} neurons triggers locomotor activation and avoidance behavior in a CRHR1-dependent manner.

CRHR1 in SN neurons does not convey effects of IPACL^{CRH} neuron activation

Next, we investigated the SN innervation by IPACL^{CRH} neurons in more detail by injecting a Cre-dependent AAV expressing Syp-mCherry into CRH-Cre::CRHR1$^{\Delta EGFP}$ mice allowing simultaneous visualization of CRH terminals and CRHR1-expressing neurons (*9*). Terminals of IPACL^{CRH} neurons were mainly found in the SN pars compacta (SNpc), additionally extending into the dorsal aspects of the SN pars reticulata (SNpr) (Fig. 6A). Single-nucleus RNA sequencing (snRNA-seq) of nuclei isolated from the ventral midbrain of CRHR1-Cre::INTACT mice revealed the presence of CRHR1 in DA, GABAergic, and glutamatergic neurons (fig. S6, A to F). Depending on their localization, SN^{CRHR1} neurons are predominantly dopaminergic (SNpc) or GABAergic (SNpr) (fig. S6, G to K). Accordingly, CRH terminals were found

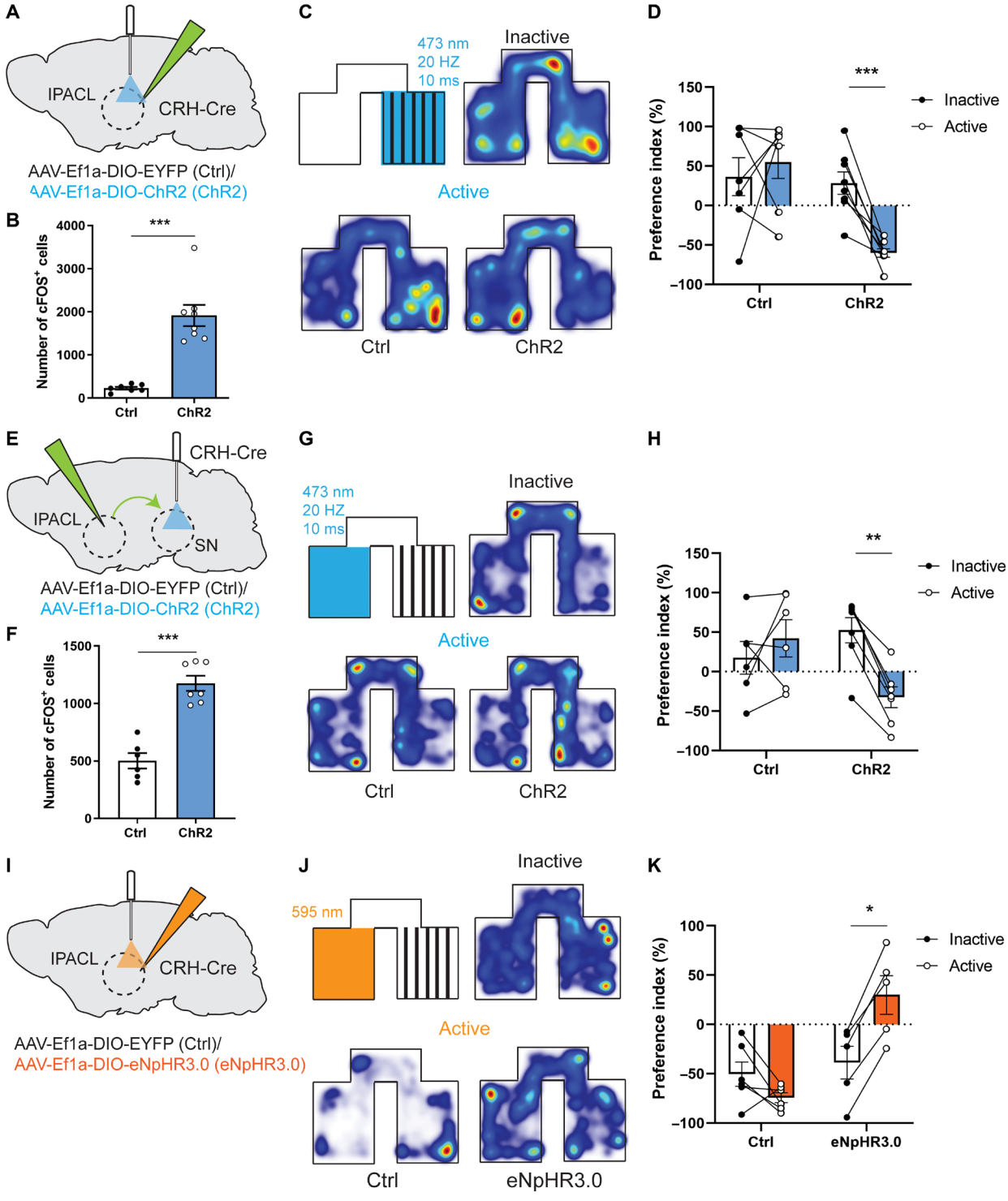

Fig. 4. Projections of IPACL^{CRH} neurons to the SN promote avoidance behavior. (**A**) Scheme illustrating injection of AAV$_5$-Ef1a-DIO-ChR2(H134R)-EYFP (ChR2) or AAV$_5$-Ef1a-DIO-EYFP (Ctrl) and placement of optic fiber in CRH-Cre mice. (**B**) Quantification of cFOS$^+$ cells in the IPACL following light activation ($P < 0.0001$, $t = 6.32$). (**C**) Scheme depicting the RTPP paradigm and heatmaps visualizing the cumulative presence of mice in the test compartments before and after light activation. (**D**) Preference index [$n = 7$ (Ctrl) and $n = 8$ (ChR2); two-way ANOVA, Bonferroni's multiple comparison, $P < 0.0001$, $t = 3.86$). (**E**) Scheme illustrating injection of AAVs into the IPACL and placement of optic fiber in the SN of CRH-Cre mice. (**F**) Quantification of cFOS$^+$ cells in the SN ($P < 0.0001$, $t = 7.13$). (**G**) RTPP paradigm with heatmaps visualizing the cumulative presence of mice in the test compartments before and during light activation. (**H**) Preference index [$n = 6$ (Ctrl) and $n = 7$ (ChR2); two-way ANOVA, Bonferroni's multiple comparison test, $P = 0.008$, $t = 3.7$]. (**I**) Scheme illustrating injection of AAV$_5$-Ef1a-DIO-eNpHR3.0-EYFP (eNpHR3.0) or AAV$_5$-Ef1a-DIO-EYFP (Ctrl) into the IPACL and placement of optic fiber in the IPACL of CRH-Cre mice. (**J**) RTPP paradigm with heatmaps visualizing the cumulative presence of mice in the test compartments before and during light inhibition. (**K**) Preference index [$n = 6$ (Ctrl) and $n = 5$ (eNpHR3.0); two-way ANOVA, Bonferroni's multiple comparison test, $P = 0.02$, t = 3.39]. Values represent means ± SEM, *$P < 0.05$, **$P < 0.01$, and ***$P < 0.0001$.

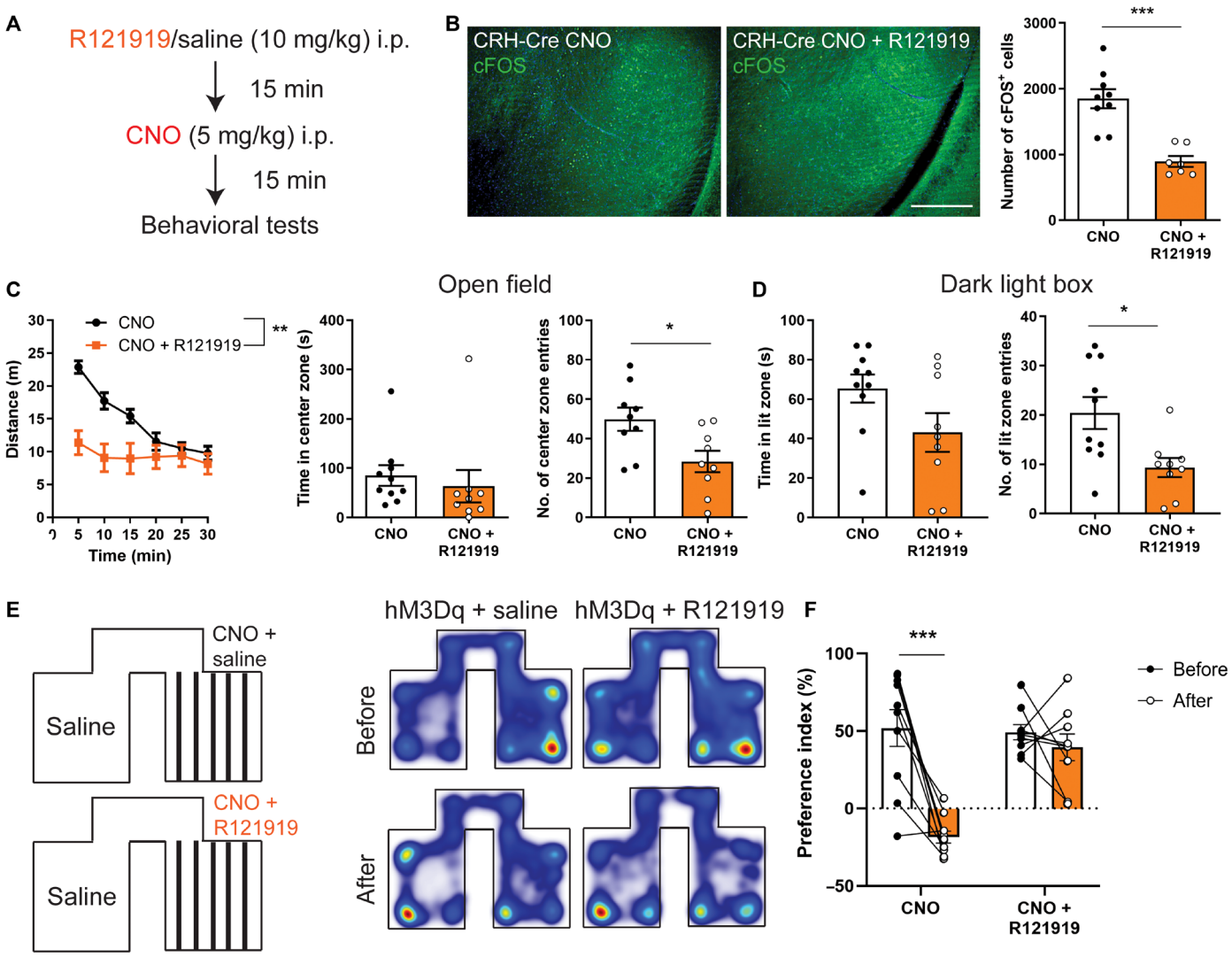

Fig. 5. IPACL^{CRH} neurons modulate locomotor activation and avoidance behavior in a CRHR1-dependent manner. (**A**) Sequential protocol used for R121919 and CNO treatment of AAV-injected CRH-Cre mice expressing hM3Dq in IPACL^{CRH} neurons. (**B**) Representative images of coronal SN sections and quantification of cFOS^{+} cells. Scale bar, 200 μm. (**C** to **F**) Treatment with the CRHR1 antagonist R121919 (10 mg/kg) blocks CNO-induced locomotor activation and avoidance behavior in mice expressing hM3Dq in IPACL^{CRH} neurons. (C) Distance traveled ($n = 9$ to 10 per group; repeated-measures two-way ANOVA, $F_{1,17} = 8.97$, $P = 0.0081$), time in center ($P = 0.57$, $t = 0.56$), and entries into center zone ($P = 0.017$, $t = 2.66$) of the open field. (D) Time spent in lit zone ($n = 9$ to 10 per group; $P = 0.12$, $t = 1.64$) and entries into lit zone ($P = 0.022$, $t = 2.54$) of the DaLi. (E) Schematic illustration of place preference paradigm and heatmaps showing the accumulated time animals stayed in respective chambers before and after conditioning. (**F**) Calculated preference index ($n = 9$ to 10 per group; two-way ANOVA, Bonferroni's multiple comparison, $P < 0.0001$, $\gamma = 5.94$). *$P < 0.05$, **$P < 0.01$, and ***$P < 0.0001$.

interspersed between tyrosine hydroxylase (TH)–positive dopaminergic and PV-positive GABAergic CRHR1^{+} neurons in the SNpc and dorsal SNpr (Fig. 6, B and C).

To directly investigate the role of CRHR1 in the SN, we activated IPACL^{CRH} neurons and simultaneously ablated CRHR1 from neurons in the SN. To this end, we expressed hM3Dq in IPACL^{CRH} neurons and injected AAV-Ef1a-Cre (+Cre) or AAV-CAG–red fluorescent protein (RFP) (+RFP) into the SN of CRH-Cre::CRHR1$^{N\text{-}EGFP}$ mice having a GFP-tagged CRHR1, which is sensitive to deletion by Cre recombinase (Fig. 6, D and E) (*9*). However, Cre-injected animals lacking CRHR1 in SN neurons were indistinguishable from control mice in all tested paradigms (Fig. 6, F to I). These results suggest that IPACL^{CRH} neurons convey locomotor activation and avoidance behavior largely independent of CRHR1 expression in SN neurons. Along these lines, chemogenetic activation of SN^{CRHR1} neurons did not reproduce the locomotor activation triggered by stimulation of IPACL^{CRH} neurons (fig. S7, A to G).

GPe^{CRHR1} neurons target the SN

These findings beg the questions to what extent IPACL^{CRH} neurons are synaptically connected with SN^{CRHR1} neurons and where CRH, potentially released following IPACL stimulation, is acting upon CRHR1. Therefore, we performed rabies virus–assisted retrograde monosynaptic tracing injecting pseudo-typed rabies virus into the SN of CRHR1-Cre animals specifically expressing avian tumor virus receptor A (TVA) in SN^{CRHR1} neurons (fig. S8A). Transsynaptic tracing revealed that SN^{CRHR1} neurons are innervated by numerous brain structures but eminently by the CeA, BNST, caudate putamen

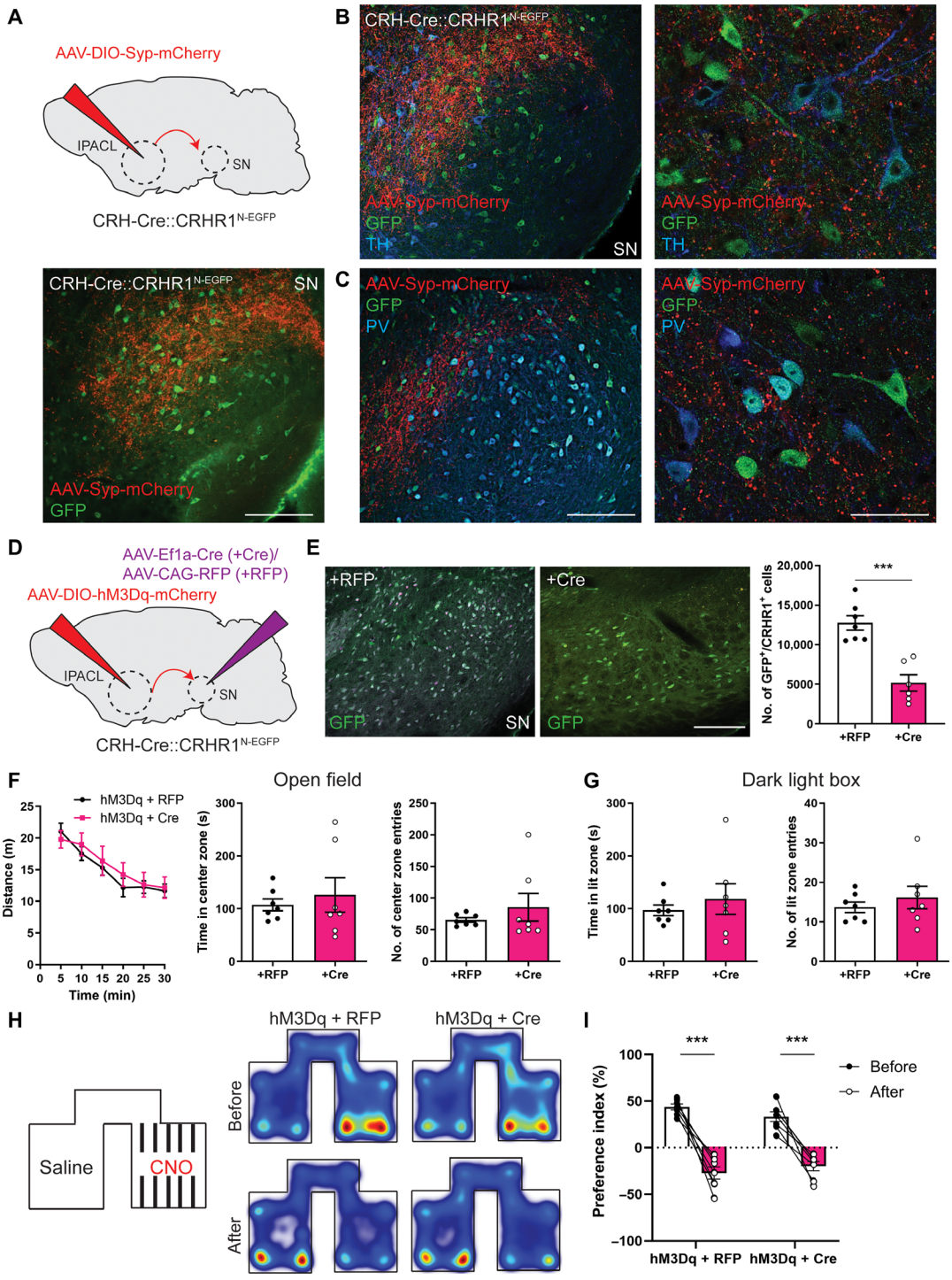

Fig. 6. IPACL^{CRH} neurons trigger locomotor activation and avoidance behavior independent of CRHR1 in the SN. (**A**) Scheme illustrating injection of AAV_8-CMV-DIO-Syp-mCherry into the IPACL of CRH-Cre::CRHR1$^{\Delta EGFP}$ mice and representative images showing terminals of IPACL^{CRH} neurons and GFP-expressing CRHR1 neurons in the SN. (**B**) Coronal SN section showing GFP-expressing CRHR1 neurons costained with the dopaminergic marker TH. (**C**) GFP-expressing CRHR1 neurons costained with the GABAergic marker PV. Images to the right show higher magnification. (**D**) Scheme illustrating coinjection of AAV_8-hSyn-DIO-hM3Dq-mCherry into the IPACL and AAV_1-Ef1a-Cre or AAV_1-CAG-RFP into the SN of CRH-Cre::CRHR1$^{N\text{-}EGFP}$ mice. (**E**) Representative images of neurons in the SN stained for GFP/CRHR1. Quantification of GFP/CRHR1 neurons in the SN ($P < 0.0001$, $t = 6.15$). (**F** to **I**) CNO treatment does not affect locomotor activation or avoidance behavior in hM3Dq-expressing animals lacking CRHR1 in the SN. (F) Distance traveled ($\gamma = 7$ per group; repeated-measures two-way ANOVA, $F_{1,12} = 0.12$, $P = 0.74$), time in center zone ($P = 0.59$, $t = 0.55$) and entries into center zone ($P = 0.38$, $t = 0.91$) of the OF. (G) Time in lit zone ($n = 7$ per group; $P = 0.49$, $t = 0.69$) and entries into lit zone ($P = 0.45$, $t = 0.77$) of the DaLi. (H) CPP paradigm with heatmaps visualizing the cumulative presence of mice in the test compartments before and after CNO treatment. (I) Preference index ($n = 7$ per group; repeated-measures two-way ANOVA, $F_{1,12} = 108.2$, $P < 0.0001$). Values represent means ± SEM, ***$P < 0.0001$. Scale bars, 200 μm.

(CPu), and GPe, whereas the IPACL showed only minor direct synaptic contacts with SN^{CRHR1} neurons (fig. S8, B, C, and F). To gain a more comprehensive view of SN afferent connections, we performed rabies virus tracing, injecting Flp-dependent AAV-CBh-fDIO-TVA-2A-GFP-OG into Vgat-FlpO (SN^{GABA} neurons) or TH-FlpO mice (SN^{DA} neurons) (fig. S8A). Most neurons projecting to SN^{DA} and SN^{GABA} neurons were detected in the CPu and the GPe, structures that are largely devoid of CRH-expressing neurons (fig. S8, B, D, E, G, and H). However, the CPu and particularly the GPe are rich in CRHR1-expressing neurons (*38*). As a major component of the basal ganglia circuit, the GPe is strongly interconnected with the SN. We observed that a large proportion of GPe^{CRHR1} neurons co-express PV (fig. S9, A and B), and anterograde tracing by injecting AAV-Ef1a-DIO-Syp-mCherry into the GPe of CRHR1-Cre animals demonstrated that GPe^{CRHR1} neurons send strong direct efferents into the SNpr (movie S5). Specifically, these GABAergic $GPe^{CRHR1/PV}$ long-range projection neurons show strong innervation of $SNpr^{PV}$ neurons in the SN (fig. S9, C and D). This was further substantiated using retrograde tracing by injecting pseudo-typed rabies virus into the SN of PV-Cre animals resulting in predominant labelling of neurons in the GPe and CPu (fig. S9, E and F). These findings raise the intriguing possibility that presynaptic CRHR1 located on GPe^{CRHR1} efferents might be the principal recipient of CRH released from $IPACL^{CRH}$ neuron terminals in the SN.

Presynaptic CRHR1 in GPe neurons conveys behavioral effects of $IPACL^{CRH}$ neuron activation

We probed whether stimulation of GPe^{CRHR1} neurons is capable of affecting locomotion and avoidance behavior. First, we used Cre-dependent AAVs to express hM3Dq or mCherry in the GPe of CRHR1-Cre animals to specifically activate GPe^{CRHR1} neurons (Fig. 7, A to C). Similar to CNO-mediated activation of $IPACL^{CRH}$ neurons, chemogenetic activation of GPe^{CRHR1} neurons triggered locomotion and avoidance behavior as observed in the OF, DaLi, and CPP (Fig. 7, D to G). Moreover, we virally expressed ChR2 in GPe^{CRHR1} neurons to demonstrate that locally confined optogenetic stimulation of GPe^{CRHR1} terminals in the SN was sufficient to activate neurons (Fig. 7, H to J) and to trigger place avoidance (Fig. 7, K and L).

To further corroborate an interaction between IPACL-SN and GPe-SN circuits, we investigated the convergence of presynaptic terminals originating from $IPACL^{CRH}$ and GPe^{CRHR1} neurons within the SN. Application of AAV-hSyn-CreOff/FlpOn-EYFP into the IPACL and AAV-hSyn-DIO-mCherry into the GPe of CRH-FlpO::CRHR1-Cre animals revealed that axon terminals of $IPACL^{CRH}$ and GPe^{CRHR1} neurons are located in close proximity within the SN, spatially enabling activation of presynaptic CRHR1 by CRH released from $IPACL^{CRH}$ neuron terminals (Fig. 8A). To test this hypothesis, we activated $IPACL^{CRH}$ neurons and simultaneously deleted CRHR1 from GPe^{CRHR1} neurons using CRH-Cre::$CRHR1^{N\text{-}EGFP}$ mice injected with AAV-hSyn-DIO-hM3Dq in the IPACL and AAV-Ef1a-Cre in the GPe (Fig. 8, B to D). Mice with a Cre-mediated deletion of CRHR1 from GPe^{CRHR1} neurons did not show any locomotor activation in the OF and DaLi following CNO application (Fig. 8, F and G, and fig. S10, A and B). Accordingly, cFOS expression was also markedly reduced in the GPe (Fig. 8E). Similarly, place avoidance behavior previously seen following activation of $IPACL^{CRH}$ neurons was prevented (Fig. 8, H and I). In contrast, neither deletion of CRHR1 from GPe^{CRHR1} neurons per se nor unspecific effects of Cre expression entailed any behavioral alterations in the OF or DaLi (fig. S10, C to E). To rule out that GPe^{CRHR1} neurons receive direct synaptic input from $IPACL^{CRH}$ neurons, we conducted rabies tracing in the GPe of CRHR1-Cre animals. While retrogradely labeled cells were observed in multiple brain regions, we only occasionally detected isolated $mCherry^{+}$ cells in the IPACL (fig. S11, A to C).

$IPACL^{CRH}$ and GPe^{CRHR1} neurons synergistically modulate neuronal activity in the SN

To interrogate the connectivity of the IPACL-SN-GPe circuit functionally, we performed in vivo calcium imaging in the SN while chemogenetically stimulating $IPACL^{CRH}$ neurons and/or optogenetically stimulating GPe^{CRHR1} terminals. Therefore, we virally expressed Flp-dependent hM3Dq in the IPACL, Cre-dependent ChrimsonR in the GPe, and GCaMP6s in the lateral SN of CRH-FlpO::CRHR1-Cre animals (Fig. 9A and fig. S12A). Following CNO application, mice were subjected to a 25-min OF with continuous recording (Fig. 9, B and C). In accordance with previously determined kinetics of CNO treatment in the OF (compare figs. S2B and S10B), we discerned basal, light-only, light + CNO, and CNO-only phases of activation. Mice showed behavioral activation following CNO and light application as evidenced by increased locomotor activity (Fig. 9C). We recorded 125 cells in total, with specific populations of cells (50%) remaining active during different conditions and cells, which were recruited during different phases of stimulation (Fig. 9D and fig. S12, B to E). We observed significantly increased neuronal activity by activation of GPe^{CRHR1} terminals (light) and by activation of both $IPACL^{CRH}$ neurons and GPe^{CRHR1} terminals (light + CNO) (Fig. 9, D to F). Activation of $IPACL^{CRH}$ neurons alone (CNO) did not induce any differences in neuronal activity compared to basal conditions potentially due to exhaustion of the sensor at the end of the imaging session (Fig. 9D). Nevertheless, we detected significantly more event counts for all three experimental conditions compared to baseline (Fig. 9, E and G). Along those lines, we performed control experiments demonstrating that individual CNO-mediated stimulation of $IPACL^{CRH}$ neurons promotes an activation of neurons comparable to optogenetic stimulation of GPe^{CRHR1} terminals in the SN (fig. S13, A to D). Together, our calcium imaging data support a functional link between $IPACL^{CRH}$ and GPe^{CRHR1} neurons governing neuronal activity in the SN.

DISCUSSION

Here, we identified and characterized a previously unidentified tripartite CRH circuit consisting of GABAergic $IPACL^{CRH}$ and GPe^{CRHR1} neurons whose efferents converge in the SN. We provide functional evidence delineating its central role in driving locomotor activation and avoidance behavior. Chemogenetic stimulation of $IPACL^{CRH}$ neurons triggered behavioral activation, particularly evidenced by increased locomotor activity. Comparable behavioral effects have been reported from early studies in the CRH field using central administration of exogenous CRH. In rats, CRH has been shown to produce dose-dependent locomotor activation and behavioral changes consistent with increased emotionality (*7*, *39*). We were able to block the behavioral alterations by systemic administration of the small-molecule antagonist R121919, which is in line with those earlier studies showing that activating effects of centrally administered CRH are fully abolished in CRHR1 knockout mice or by coadministration of the peptide antagonist α-helical $CRH_{9–41}$ (*19*, *40*). The effect of CRH on behavioral arousal and locomotor activity is highly

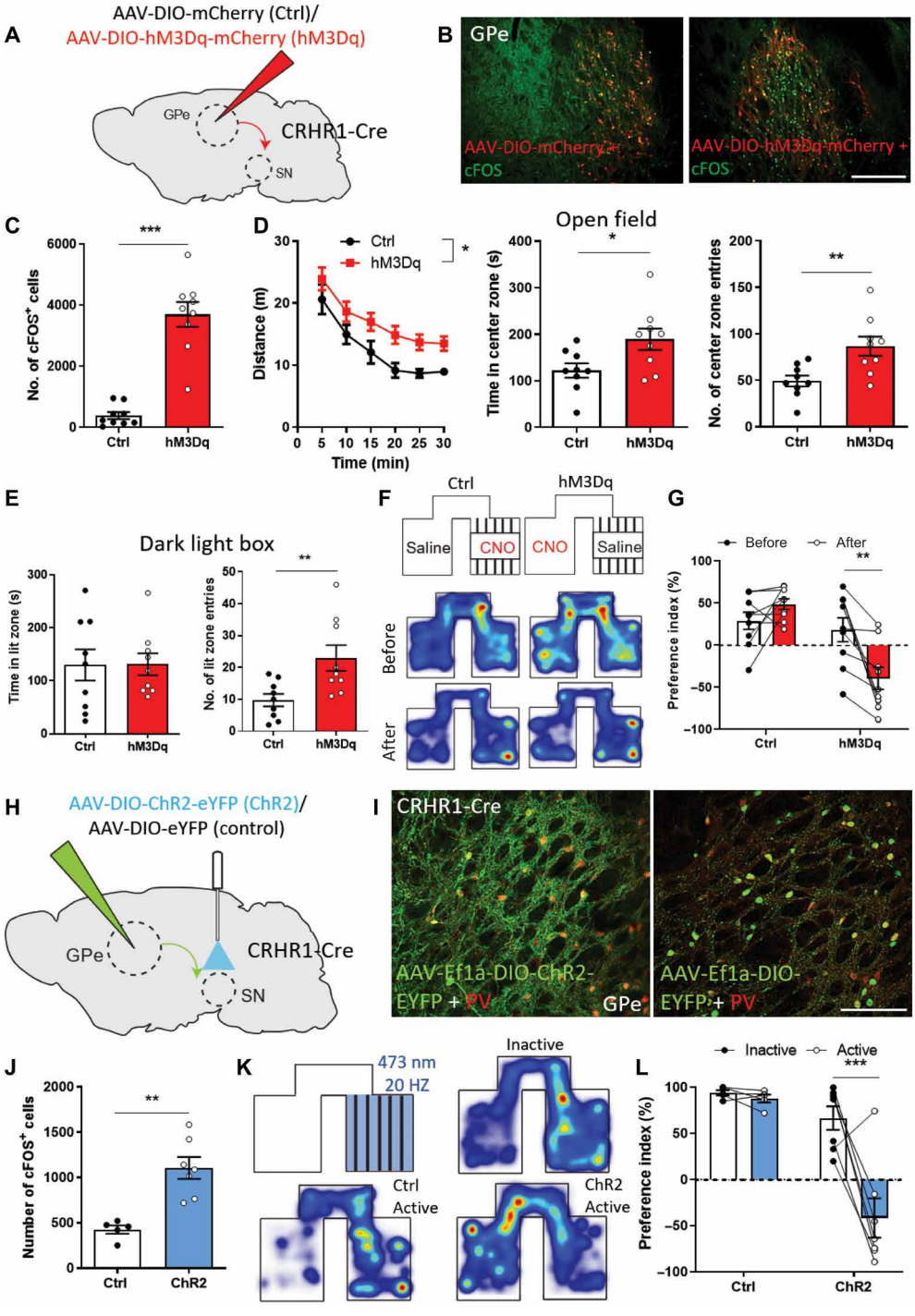

Fig. 7. Stimulation of GPe^{CRHR1} neurons promotes locomotor activation and avoidance behavior. (**A**) Scheme illustrating injection of AAV_8-hSyn-DIO-hM3Dq-mCherry (hM3Dq) or AAV_8-hSyn-DIO-mCherry (Ctrl) into the GPe of CRHR1-Cre mice. (**B**) Representative coronal GPe sections stained for cFOS and (**C**) quantification of cFOS$^+$ cells 90 min following CNO administration ($P < 0.0001$, $t = 7.81$). (**D** to **G**) CNO-mediated activation of GPe^{CRHR1} neurons induces locomotor activation, delayed habituation, and avoidance behavior in hM3Dq-expressing animals ($n = 9$ animals per group in all paradigms). (D) Distance traveled (repeated-measures two-way ANOVA, $F_{1,14} = 6.54$, $P = 0.022$), time spent in the center zone ($P = 0.027$, $t = 2.43$), and entries into the center zone ($P = 0.006$, $t = 3.15$) of the OF. (E) Time spent in the lit zone ($P = 0.95$, $t = 0.04$) and entries into the lit zone ($P = 0.009$, $t = 2.94$) of the DaLi. (F) CPP paradigm with heatmaps visualizing the cumulative presence of mice in the test compartments before and after CNO treatment. (G) Preference index two-way ANOVA, Bonferroni's multiple comparison test, $P = 0.006$, $t = 3.59$. (**H**) Scheme illustrating injection of AAV_5-Ef1a-DIO-ChR2-EYFP (ChR2) and AAV_5-Ef1a-DIO-EYFP (Ctrl) into the GPe of CRHR1-Cre mice. (**I**) Representative images of coronal GPe sections from AAV-injected CRHR1-Cre mice stained for PV and cFOS. (**J**) Quantification of cFOS$^+$ cells in the SN following light-induced activation of ChR2-expressing GPe^{CRHR1} neuron terminals in the SN ($P = 0.001$, $t = 4.56$). (**K**) RTPP paradigm with heatmaps visualizing the cumulative presence of mice in the test compartments before and after light activation. (**L**) Preference index [$n = 5$ (Ctrl) and $n = 7$ (ChR2) animals per group; two-way ANOVA, Bonferroni's multiple comparison test, $P < 0.0001$, $t = 5.56$). Values represent means ± SEM, $^*P < 0.05$, $^{**}P < 0.01$, and $^{***}P < 0.0001$. Scale bars, 200 μm.

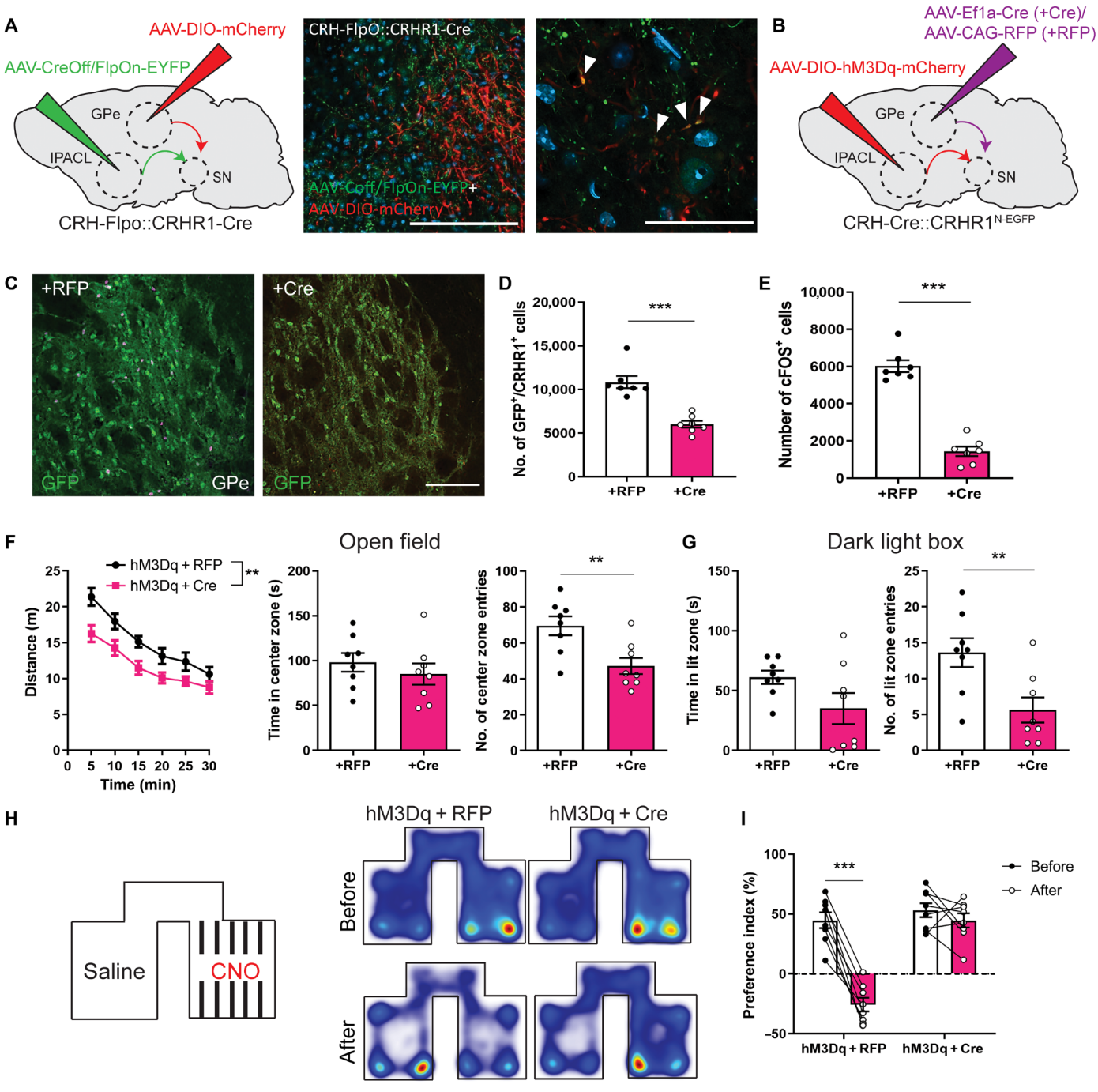

Fig. 8. CRHR1 on GPe^{CRHR1} neuron terminals is required for locomotor activation and avoidance behavior driven by IPACL^{CRH} neurons. (**A**) Scheme displaying coinjection of AAV$_{DJ}$-hSyn-CreOff/FlpOn-EYFP into the IPACL and AAV$_8$-hSyn-DIO-mCherry into the GPe of CRH-FlpO::CRHR1-Cre mice and representative images showing terminals of IPACL^{CRH} and GPe^{CRHR1} neurons in the lateral SN. Scale bar, 100 μm (right). White arrowheads indicate colocalization of IPACL^{CRH} and GPe^{CRHR1} neuron terminals. (**B**) Scheme illustrating coinjection of AAV$_8$-hSyn-DIO-hM3Dq-mCherry in the IPACL and AAV$_1$-Ef1a-Cre or AAV$_1$-CAG-RFP in the GPe of CRH-Cre::CRHR1$^{N\text{-}EGFP}$ mice. (**C**) Representative images of neurons in the GPe stained for GFP/CRHR1. (**D**) Quantification of GFP/CRHR1 neurons in the GPe ($P < 0.0001$, $t = 6.15$). (**E**) Quantification of cFOS$^+$ cells 90 min following CNO administration in the GPe ($P = 0.0002$, $\gamma = 5.53$). (**F** to **I**) Ablation of CRHR1 from GPe^{CRHR1} neurons reduces locomotor activation and avoidance behavior induced by CNO treatment in hM3Dq-expressing animals. (F) Distance traveled ($n = 8$ animals per group; repeated-measures two-way ANOVA, $F_{1,14} = 9.26$, $P = 0.0088$), time in center zone ($P = 0.42$, $t = 0.83$), and entries into center zone ($P = 0.006$, $t = 3.21$) of the OF. (G) Time in lit zone ($n = 8$ animals per group; $P = 0.087$, $t = 1.84$) and entries into lit zone ($P = 0.0095$, $t = 3$) of the DaLi. (H) CPP paradigm with heatmaps visualizing the cumulative presence of mice in the test compartments before and after CNO treatment. (I) Preference index ($n = 8$ animals per group; two-way ANOVA, Bonferroni's multiple comparison test, $P < 0.0001$, $t = 8.23$). $^{**}P < 0.01$ and $^{***}P < 0.0001$.

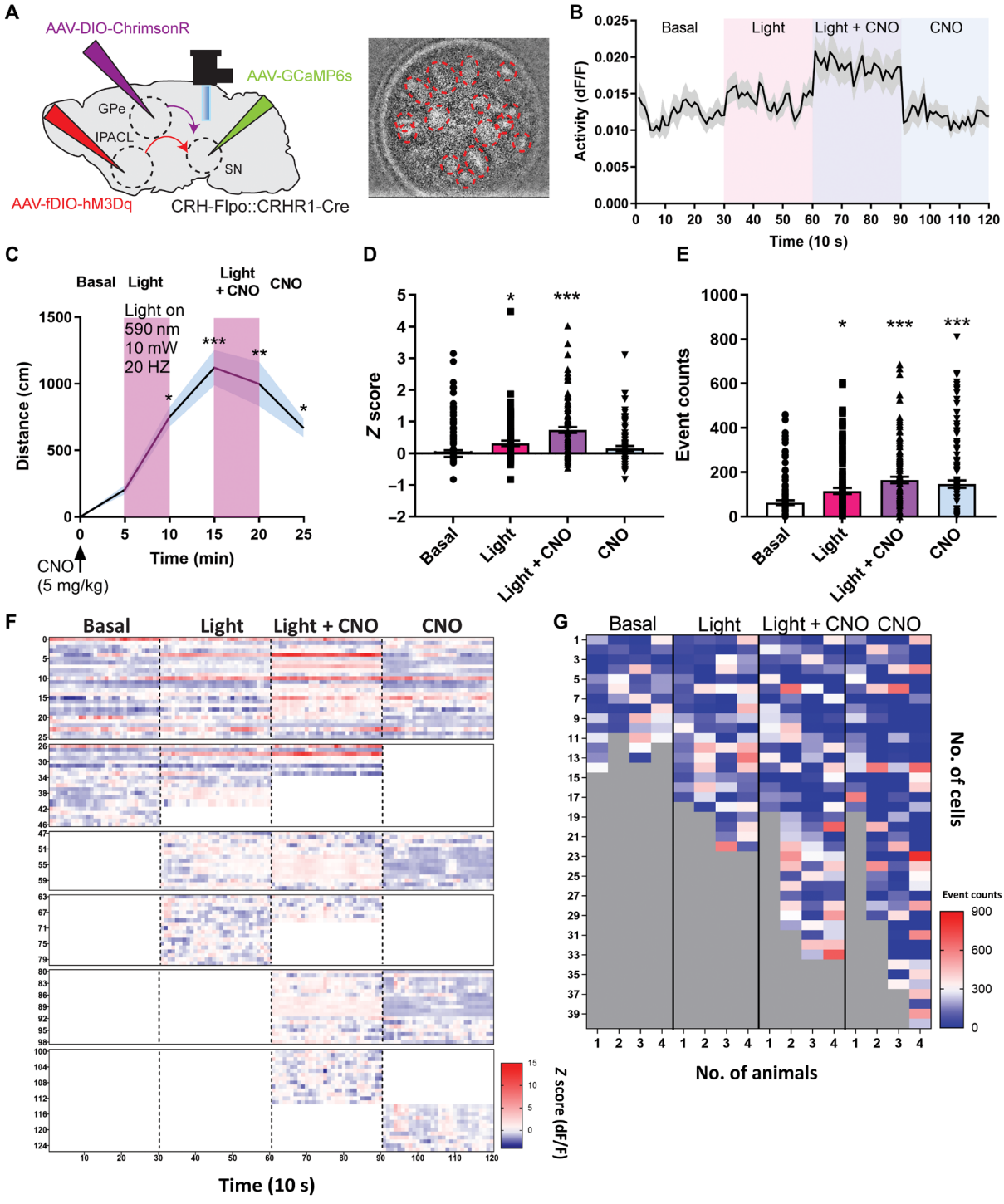

Fig. 9. IPACL^{CRH} and GPe^{CRHR1} neurons synergistically modulate neuronal activity in the SN. (**A**) Scheme displaying injection of AAV_8-hSyn-fDIO-hM3Dq-mCherry into the IPACL (enables chemogenetic stimulation of IPACL^{CRH} neurons), AAV_8-hSyn-DIO-ChrimsonR-tdTomato into the GPe (enables optogenetic stimulation of GPe^{CRHR1} neurons), and AAV5-hSyn-GCaMP6s into the SN (enables imaging of neuronal activity) and of gradient index (GRIN) lens above the lateral SN (enables imaging of SN neurons and stimulation of GPe^{CRHR1} terminals) of CRH-FlpO::CRHR1-Cre mice. Representative image showing cells with fluorescence signal as detected by the miniscope (encircled by red dashed lines). (**B**) Representative activity traces of one of the identified clusters showing cells active throughout the recording session. (**C**) Locomotor activity of mice subjected to different stimulation regimes ($n = 4$ animals per group; one-way ANOVA, Bonferroni's multiple comparison test, light, $P = 0.01$; CNO, $P < 0.0001$; light + CNO, $P = 0.002$; CNO, $P = 0.036$). (**D**) Cell activity under different stimulation regimes compared to basal conditions (one-way ANOVA, Bonferroni's multiple comparison test, light, $P = 0.033$; light + CNO, $P < 0.0001$; CNO, $P = 0.265$). (**E**) Event counts following different stimulations compared to basal conditions (one-way ANOVA, Bonferroni's multiple comparison test, Light, $P = 0.027$; light + CNO, $P < 0.0001$; CNO, $P = 0.0001$). (**F**) Heatmap visualization of cell activities active during different conditions. (**G**) Heatmap visualization of event counts during different conditions. Values represent means ± SEM, $^*P < 0.05$, $^{**}P < 0.01$, and $^{***}P < 0.0001$.

conserved among vertebrates (*6*). Unexpectedly, neither the respective sites within the central nervous system that mediate the CRH-induced increase in locomotor activity nor the endogenous CRH source have been identified yet. Behavioral activation can be differentiated into nonambulatory motor activity and ambulatory locomotion. Along these lines, local administration of CRH into the locus coeruleus (LC) has been proven to activate spontaneous nonambulatory motor activity, while ambulatory (i.e. locomotor) activity remained unaffected. In the forced swim test, which addresses arousal and agitation in a stressful situation, LC-confined CRH application resulted in significant behavioral activation reflected by reduced immobility (*17*). Previous studies suggesting regions of the ventral forebrain as relevant for CRH-induced locomotor activity (*41*) have been contradicted by findings from intra-VTA injection of CRH, which have shown to dose-dependently increase horizontal and vertical activity compared to vehicle injected animals. Notably, the minimal effective CRH dose to reach similar effects via injection in the lateral ventricle was 30 times higher compared to the intra-VTA injection (*42*).

Besides the profound behavioral effects (*43*), centrally administered CRH also triggers other physiological processes characteristic of a stress response, including activation of the HPA axis and of the sympathetic nervous system, which are part of the body's arousal system. The enhanced activation of the HPA axis advocates that stimulation of IPACL^{CRH} neurons is perceived as stressful and aversive. Therefore, it is highly likely that other measures of arousal are also increased upon stimulation of IPACL^{CRH} neurons as it has been observed following central application of exogenous CRH. The aversiveness of IPACL^{CRH} neuron stimulation is supported by the results obtained from the CPP and RTPP paradigms, which show that chemogenetic or optogenetic stimulation of IPACL^{CRH} neurons or their efferents in the SN consistently produce avoidance behavior. This is in line with previous studies demonstrating that centrally applied CRH induces place aversion in a place conditioning paradigm (*44*). In this context, it is of interest that the IPAC has recently been identified to control aversive responses in the context of innate and learned disgust, suggesting a more general role of this brain region in expression of aversive behaviors (*45*).

Presynaptically localized CRH receptors and the capacity of presynaptic CRHR1 to facilitate GABA release have already been demonstrated (*46*–*49*). Similarly, it has been proven that presynaptic CRHR1 and CRHR2 are tightly regulating glutamate transmission in the VTA in a concerted and heterosynaptic manner (*50*). Accordingly, our data suggest that GABA release from GPe^{CRHR1} neurons is triggered by direct neuronal stimulation and further facilitated by presynaptic CRHR1 activated by CRH released from IPACL^{CRH} efferents in the SN. Analogous to other G protein–coupled receptors (*51*), presynaptic CRHR1 has the capacity to provide the means for local modulation and control of neuronal communication. Thus, CRH might enable long-lasting tuning of GPe^{CRHR1} neurons to set the gain of these cells based to the behavioral state but might also be altered in stress-related pathologies.

We found that most GPe^{CRHR1} neurons express PV. This subpopulation of GPe neurons directly innervates the SNpc and SNpr (*52*–*54*). Along these lines, we observed that GPe^{CRHR1} neurons predominantly form synapses at perikarya and primary dendrites of inhibitory SNpr^{PV} cells, which represent a major output of the basal ganglia circuit (*55*). Optogenetic or chemogenetic activation of SNpr basal ganglia output neurons has been shown to impair spontaneous locomotion and to block active avoidance (*56*, *57*). In contrast, inhibition of SNpr neurons facilitates avoidance behavior (*57*). This is in agreement with our observation that stimulation of IPACL^{CRH} or GPe^{CRHR1} neurons, likely resulting in inhibition of SNpr projection neurons, promotes avoidance behavior in the applied place preference paradigms. In parallel, enhanced inhibition of GABAergic output neurons might also disinhibit the inhibitory drive on SNpc^{DA} neurons, which is conveyed via axon collaterals of SNpr output neurons (*58*). It remains to be investigated to what extent stimulation of IPACL^{CRH} neurons directly affects DA release, which might further contribute to the observed hyperlocomotion. Only recently, another extended amygdala–basal ganglia circuit has been described connecting the CeA and the lateral SN contributing to emotional behaviors involving appetitive and aversive learning (*59*). Considering the abundance of CRH neurons in the CeA, it is highly likely that CeA^{CRH} neurons also contribute to this circuit, potentially interacting with the tripartite circuit identified in this study. The SN has classically been regarded as part of the basal ganglia motor circuit controlling voluntary movements. However, accumulating evidence, including our findings, contradict a clear anatomical and functional segregation of midbrain DA systems (*60*).

Our results corroborate the notion that the identified CRH system–related extended amygdala–basal ganglia circuit at least partially accounts for the well-established effects of CRH on behavioral arousal and locomotor activity. In view of these results, it is tempting to speculate that this circuit might contribute to pathological hyperarousal and maladaptive avoidance responses, which are hallmarks of anxiety and depression.

MATERIALS AND METHODS

Mice

All animal experiments were conducted with the approval of and in accordance to the Guide of the Care and Use of Laboratory Animals of the Government of Upper Bavaria, Germany. Mice were group-housed under standard laboratory conditions (22° ± 1°C, 55 ± 5% humidity) and maintained under a 12-hour light/12-hour dark cycle with food and water ad libitum. All experiments were conducted with adult male mice (age, 2 to 5 months). The following mouse lines were used: CRH-Cre (*Crh*$^{tm1(cre)Zjh}$; the Jackson Laboratory, stock no. 012704) (*61*), CRH-FlpO (*Crh*$^{tm1.1(flpo)Bsab}$; the Jackson Laboratory, stock no. 031559) (*62*), CRHR1-Cre (*Crhr1*$^{tm4.1(cre)Jde}$) (*13*), CRHR1$^{\Delta-EGFP}$ (*Crhr1*^{tm1Jde}) (*9*), CRHR1^{N-EGFP} (*Crhr1*$^{tm1.1Jde}$) (*9*), PV-Cre (*Pvalb*$^{tm1(cre)Arbr}$) (*63*), TH-FlpO (*Th*$^{tm1.1(flpo)Awar}$) (*64*), Vgat-FlpO (*Slc32a1*$^{tm1.1(flpo)Hze}$; the Jackson Laboratory, stock no. 029591) (*65*), INTACT [*Gt(ROSA)26Sor*$^{tm5(CAG-Sun1/sfGFP)Nat}$; the Jackson Laboratory, stock no. 021039] (*66*), Ai9 [*Gt(ROSA)26Sor*$^{tm9(CAG-tdTomato)Hze}$, the Jackson Laboratory, stock no. 007909] (*67*), and Ai65 [*Gt(ROSA)26Sor*$^{tm65.1(CAG-tdTomato)Hze}$; the Jackson Laboratory stock no. 021875] (*68*). The following double and triple transgenic lines were generated in this study by cross-breeding of single transgenic lines: CRH-Cre::Ai9, CRH-Cre::Vgat-FlpO::Ai65, CRH-Cre::CRHR1$^{\Delta-EGFP}$, CRH-Cre::CRHR1^{N-EGFP}, CRH-FlpO::CRHR1-Cre, and CRHR1-Cre::INTACT. Primer sequences and protocols for genotyping are available upon request.

Electrophysiology

Eight- to 12-week-old CRH-Cre::Ai9 mice were anesthetized with isoflurane and decapitated. The brain was rapidly removed from the cranial cavity and, using a vibratome (HM650V, Thermo Fisher Scientific), 350-μm-thick coronal slices containing the IPACL were cut

in an ice-cold carbogen gas–saturated (95% O_2/5% CO_2) solution consisting of the following: 87 mM NaCl, 2.5 mM KCl, 25 mM $NaHCO_3$, 1.25 mM NaH_2PO_4, 0.5 mM $CaCl_2$, 7 mM $MgCl_2$, 10 mM glucose, and 75 mM sucrose. Slices were incubated in carbogenated physiological saline for 30 min at 34°C and, afterward, for at least 30 min at room temperature (23° to 25°C). The physiological saline contained the following: 125 mM NaCl, 2.5 mM KCl, 25 mM $NaHCO_3$, 1.25 mM NaH_2PO_4, 2 mM $CaCl_2$, 1 mM $MgCl_2$, and 10 mM glucose. In the recording chamber, slices were superfused with carbogenated physiological saline (flow rate at 2 to 3 ml/min), and CRH^+ and CRH^- IPACL neurons were identified using epifluorescence and infrared videomicroscopy. Somatic whole-cell current- and voltage-clamp recordings (−70-mV holding potential, >1-gigohm seal resistance, <20-megohm series resistance, 3-kHz low-pass filter, and 15-kHz sampling rate) were performed at room temperature using an EPC 10 amplifier (HEKA). For current-clamp measurements, patch pipettes (3- to 5-megohm open tip resistance) were filled with a solution consisting of the following: 135 mM $KMeSO_4$, 8 mM NaCl, 0.3 mM EGTA, 10 mM Hepes, 2 mM Mg–adenosine 5′-triphosphate (ATP), and 0.3 mM Na–guanosine 5′-triphosphate (GTP). In these experiments, NBQX (2,3-dihydroxy-6-nitro-7-sulfamoylbenzo[*f*] quinoxaline6-nitro-7-sulfamoylbenzo[*f*]quinoxaline-2,3-dione; 5 μM) and picrotoxin (100 μM) were added to the physiological saline. Current injections were used to depolarize or hyperpolarize the neuron under investigation. For voltage-clamp recordings of spontaneous AMPA receptor–mediated excitatory postsynaptic currents (AMPA-sEPSCs), the pipette solution consisted of the following: 125 mM $CsCH_3SO_3$, 8 mM NaCl, 10 mM Hepes, 0.5 mM EGTA, 4 mM Mg-ATP, 0.3 mM Na-GTP, and 20 mM Na_2-phosphocreatine. In these experiments, picrotoxin (100 μM) was added to the physiological saline. For recordings of spontaneous $GABA_A$ receptor–mediated inhibitory postsynaptic currents ($GABA_A$-sIPSCs), the pipette solution was composed of the following: 140 mM KCl, 5 mM NaCl, 10 mM Hepes, 0.1 mM EGTA, 2 mM Mg-ATP, 0.3 mM Na-GTP, and 20 mM Na_2-phosphocreatine. In these experiments, NBQX (5 μM) was added to the physiological saline. Offline analysis of electrophysiological data was performed using the Fitmaster software (HEKA) and Igor Pro program (WaveMetrics).

Immunohistochemistry

Mice were euthanized with an overdose of isoflurane (Floren, Abbott) and transcardially perfused with 20 of ml phosphate-buffered saline (PBS), followed by 20 ml of 4% paraformaldehyde (PFA). Dissected brains were postfixed in 4% PFA overnight at 4°C, and 50-μm-thick sections were prepared using a vibratome (Microm HM 650 V, Thermo Fisher Scientific). Sections were rinsed in PBS and incubated overnight at 4°C with the primary antibody in PBS with 0.5% Triton X-100. On the next day, sections were washed, incubated with the secondary antibody coupled to suitable fluorescence (1:250 Alexa Fluor; Invitrogen, Thermo Fisher Scientific), and afterward washed with PBS. Sections were mounted using Fluoromount-G mounting medium (SouthernBiotech) and either left to air-dry or stored at −20°C for image acquisition. The primary antibodies used were as follows: rabbit anti-CRH (1:10,000; obtained from P. E. Sawchenko; Salk Institute, CA), chicken anti-GFP antibody (1:500; Aves), rabbit anti-TH antibody (1:1000; Millipore), mouse anti-PV antibody (1:500; Swant), rabbit anti-RFP antibody (1:500; Rockland), rabbit anti-cFOS antibody (1:1000; Abcam), rabbit anti-WFS1 (1:200; St John's Laboratory), mouse anti-CALB (1:500; Sigma-Aldrich), rabbit anti-SOM (1:500; Peninsula Laboratories International), rabbit anti-calretinin (1:1000; SYSY), and mouse anti-Pkcd (1:200; BD Biosciences). For quantification, all slides were randomized and coded before quantitative analysis. TH-, PV-, and cFOS-labeled cells were counted on every sixth section through the entire rostrocaudal extent of regions of interest (ROIs; six sections per animal). Images were captured with either a Zeiss Axioplan2 fluorescence microscope and Axio Vision 4.5 software or a Zeiss inverted laser scanning confocal microscope and Zen software. For confocal imaging, a z-stack of pictures of areas of interest was obtained with 0.4- to 1.2-μm step size and 800-pixel by 800-pixel to 1024-pixel by 1024-pixel picture size. Images were analyzed with ImageJ (https://imagej.nih.gov/ij/).

Double ISH

Brains were sectioned coronally at 20 μm using a cryostat (Microm, Walldorf, Germany). The sections were thaw-mounted onto SuperFrost slides, dried, and kept at −80°C. Single and double ISH was performed as previously described (*13*). The following riboprobes were used: CRH (3′ untranslated region), 2108 to 2370 base pairs (bp) of AY128673; Tomato, 740 to 1428 bp of AY678269. Quantifications of ISHs were performed blindly using the freely available NIH ImageJ software (https://imagej.nih.gov/ij/).

CLARITY

Perfused mouse brains were fixed in 4% PFA overnight and then transferred into 1% hydrogel solution (1% acrylamide, 0.0125% bis-acrylamide, 4% PFA, and 0.25% VA-044 initiator) for 48 hours. The samples were degassed (nitrogen replacing oxygen, using 50-ml caps with tubing for 30 min) and polymerized (overnight at 37°C) in a 50-ml tube. Brains were removed from hydrogel and washed with 200 mM NaOH–boric acid buffer (pH 8.5) containing 8% SDS for 12 hours at 37°C (without shaking) to remove residual PFA and monomers. Brains were transferred to a flow-assisted clearing device using a temperature-control circulator. Next, 100 mM tris-boric buffer (pH 8.5) containing 8% SDS was used to accelerate the clearing (at 37° to 40°C). After clearing, the brains were washed in PBS with 0.2% Triton X-100 for at least 48 hours at 37°C to remove residual SDS. Brains were incubated in sorbitol refractive index matching solution for several days at room temperature and then subjected to imaging using a LaVision Light Sheet microscope (LaVision BioTec, Duisburg, Germany).

Isolation and snRNA-seq

Mice were euthanized at 2 months of age by cervical dislocation. Brains were collected in ice-cold PBS and processed for tissue dissection. The target region (ventral midbrain) was isolated by subjecting brains to a brain matrix (Fine Science Tools). Brains were cut into 1-mm thick slices covering the entire ROI. The dorsal part including the cortex was removed, and the remaining tissue was homogenized in 2 ml of lysis buffer [0.32 M sucrose, 10 mM tris (pH 8.0), 5 mM $CaCl_2$, 3 mM Mg acetate, 1 mM dithiothreitol (DTT), 0.1 mM EDTA, and 0.1% Triton X-100] by douncing 10 to 50 times in a 7-ml dounce homogenizer. Lysate was transferred to a 4-ml ultracentrifugation tube (Beckman, 344061; 14 mm by 95 mm), and 2 ml of sucrose solution [1.8 M sucrose, 10 mM tris (pH 8.0), 3 mM Mg acetate, and 1 mM DTT] was pipetted directly to the bottom of the tube. Ultracentrifugation was carried out at 24,400 rpm for 2.5 hours at 4°C (Beckman, L8-70 M, SW80 rotor). After centrifugation, the upper two layers were removed by aspiration. The nuclei pellet was resuspended in PBS with 0.1% fetal bovine serum. Then, samples

were processed to fluorescence-activated cell sorting (FACS) using a FACSMelody (Becton Dickinson) with a nozzle diameter of 100 μm and FACSFlow medium. Debris and aggregated nuclei were gated out by forward and sideward scatter. Single nuclei were gated out by FSC-width/FSC-area. Gating for fluorophores was done using isolated nuclei possessing GFP in the nuclear membrane.

snRNA-seq was performed using 10× genomics kit following the instructions of the manufacturer. Briefly, nuclei were mixed with solutions containing barcoded beads and partitioning oil. To achieve single-nucleus resolution, nuclei were delivered at a limiting dilution. Next, gel beads were dissolved, primers were released, and any copartitioned nucleus was lysed. Primers were mixed with the cell lysate and with a master mix containing reverse transcription reagents. This produced barcoded, full-length cDNA from polyadenylated mRNA. After incubation, products were broken up and pooled fractions recovered. Silane magnetic beads were used to purify the first-strand cDNA from the post–reverse transcription reaction mixture. Barcoded, full-length cDNA was amplified via polymerase chain reaction to generate sufficient mass for library construction. Enzymatic fragmentation and size selection were used to optimize the cDNA amplicon size. A Chromium Single-Cell 3′ Gene Expression library comprises standard Illumina paired-end constructs beginning and ending with P5 and P7. The 16-bp 10× barcode and 12-bp unique molecular identifier (UMI) were encoded in Read 1, while Read 2 was used to sequence the cDNA fragments. Sample index sequences were incorporated as the i7 index read. TruSeq Read 1 and TruSeq Read 2 are standard Illumina sequencing primer sites used in paired-end sequencing.

Analysis of snRNA-seq data

Single-nuclei data were analyzed using the python package SCANPY (*69*). Quality controls (QCs), including nucleus QC and gene QC, were carried out on the raw dataset. The following measures were assessed: number of UMIs, number of expressed genes, and the fraction of mitochondrial genes. Of the 492,928 nuclei and 31,053 genes in the raw dataset, 54 nuclei with gene counts greater than 3500, and 476,198 nuclei that had gene counts fewer than 200 were removed. Of these, 11 nuclei were filtered out for having a fraction of mitochondrial genes higher than 0.04. Moreover, 17,614 genes that were detected in less than 20 nuclei were filtered out. After filtering, 16,665 nuclei and 13,439 genes remained for further analysis. To normalize feature and gene counts, the R package scran (*70*) was used. A total of 4000 highly variable genes were selected after data normalization, which were used for dimensionality reduction with principal components analysis and clustering through embedding into a *k*-nearest neighbors graph using the louvain algorithm implemented in SCANPY. The clusters were visualized with the UMAP (Uniform Manifold Approximation and Projection) algorithm. To minimize the number of doublets and to ensure that nuclei did not cluster by the cell cycle phases, doublets were identified using the Python package scrublet (*71*), and nuclei at different stages in cell cycle were recognized using marker genes (*72*). A Welch *t* test was performed for differential gene expression between clusters. Cluster-specific marker genes were used to annotate each cluster.

Stereotactic surgeries

Mice were anesthetized for surgery with isoflurane (Floren, Abbott), 2% (v/v) in O_2, and placed in a stereotaxic frame (Kopf Instruments). Body temperature was maintained with a heating pad. Metacam (5 mg/kg of body weight) was administered as a systemic analgesic. Virus and tracer were delivered using a 33-gauge microinjection needle with a 2.5-μl Hamilton syringe (Hamilton) coupled to an automated microinjection pump (World Precision Instruments Inc.) at 100 nl/min. Postsurgery recovery included Metacam supplementation (5 mg/kg, subcutaneous injection) for 3 days after surgery, with daily monitoring of food intake.

Viral injections and tracing analyses

For retrograde tracing, 0.5 μl of FG (Fluorochrome LLC) were injected unilaterally in the ROI: SN [anterior-posterior (AP): −3, medial-lateral (ML): 1.65, dorsal-ventral (DV): −4.13). After incubation for 7 days, mice were euthanized for further analysis. For anterograde tracing, 0.5 μl of AAV_9-CMV-DIO-Syn-GFP, AAV_8-Ef1a-DIO-Syn-mCherry (~10^{13} vector genomes (vg)/ml; MIT Vector Core), or AAV_{DJ}-hSyn-CreOff/FlpOn-EYFP (~10^{12} vg/ml; UNC Vector Core, provided by the Deisseroth laboratory) were injected into Bed nucleus of the stria terminalis, lateral division, dorsal (BSTLD) (AP: 0.14, ML: 0.9, DV: −3.9), Bed nucleus of the stria terminalis, lateral division, posterior (BSTLP) (AP: 0.14, ML: 0.9, DV: −4.3), CeA (AP: −1.22, ML: 2.8, DV: −4.7), IPACL (AP: 0.26, ML: 2, DV: −5), or GPe (AP: −0.34, ML: 1.8, DV: −4). Viral tracers were incubated for a minimum of 2 weeks before the mice were euthanized.

For retrograde rabies virus tracing, we first injected AAV_1-CBh-DIO-TVA-T2A-GFP-OG or AAV_1-hSyn-fDIO-revTVA-t2A-GFP-OG (~10^{16} vg/ml) into SN or GPe. Two weeks later, SAD-EnVA-dG-mCherry rabies virus was injected into the same region. One week after injection of rabies virus, mice were euthanized for further analysis.

For chemogenetic experiments, 0.5 μl of virus AAV_8-hSyn-DIO-mCherry or AAV_8-hSyn-DIO-hM3Dq-mCherry (Addgene plasmid #50459 and #44361; ~10^8 vg/ml) was injected bilaterally into target regions (IPACL, SN, or GPe) using previous coordinates. For optogenetic manipulation, 0.5 μl of AAV_5-Ef1a-DIO-ChR2-EYFP, AAV_5-Ef1a-DIO-eNpHR3.0-EYFP, or AAV_5-Ef1a-DIO-EYFP virus (~10^{12} vg/ml; UNC Vector Core, provided by the Deisseroth laboratory) was injected into the IPACL. For in vivo calcium imaging experiments, AAV_8-hSyn-fDIO-hM3Dq-mCherry (~10^{16} vg/ml) was injected into the IPACL, AAV_8-hSyn-FLEX-ChrimsonR-tdTomato (~10^{12} vg/ml; UNC Vector Core) in the GPe and $AAV_{2/1}$-hSyn-GCaMP6s (~10^{12} vg/ml; UPenn Vector Core) in the SN. In general, mice were allowed to recover for at least 2 weeks before entering behavioral experiments.

Placement of optic fiber

Two weeks after virus injection, an optic fiber (200-μm core, 0.39 numerical aperture, 1.25 mm ferrule; Thorlabs) was implanted bilaterally above the IPACL (AP: 0.26, ML: 2, DV: −4.7 mm) or SN (AP: −3, ML: 1.65, DV: −3.8 mm). Implants were secured with cyanoacrylic glue (Braun), and the exposed skull was covered with dental acrylic (Paladur, Heraeus). The animals were left for 2 weeks for recovery before subjecting them to the RTPP.

Behavioral assays

Mice were single-housed for a week and entered the respective test apparatus in random order. Mice rested for 1 day between each behavioral test, except in the conditioned place preference test. All experiments were analyzed using the automated video tracking system ANYmaze (Stoelting, Wood Dale, IL) and Ethovision (Noldus, Wageningen).

For chemogenetic activation of neurons, CNO dihydrochloride was dissolved in 0.9% saline at a concentration of 2.5 mg/ml. CNO was

administered through intraperitoneal injection (5 mg/kg) 15 min before mice entered the behavioral test apparatus. For blockade of CRHR1, R121919 (*73*) hydrochloride was dissolved in 0.9% saline with 5% of ethanol at a concentration of 1.25 mg/ml. R121919 was administered through intraperitoneal injection (10 mg/kg) 30 min before each behavioral test.

The OF test was conducted in an evenly illuminated (<15 lx) square apparatus [40 cm (*l*) by 40 cm (*w*) by 60 cm (*h*)]. The test duration was 30 or 90 min. The 15-min DaLi box test was performed in an apparatus consisting of a secure black compartment [10 cm (*l*) by 20 cm (*w*) by 35 cm (*h*), <5 lx] and an aversive, brightly illuminated white compartment [10 cm (*l*) by 20 cm (*w*) by 35 cm (*h*), 400 lx] connected by a tunnel.

The CPP apparatus [T shape, 40 cm (*l*) by 40 cm (*w*) by 35 cm (*h*)] consisted of a starting box and two conditioning boxes made of black acrylic boards. The conditioning compartments [18 cm (*l*) by 20 cm (*w*) by 35 cm (*h*)] were separated by a smaller compartment [10 cm (*l*) by 20 cm (*w*) by 35 cm (*h*)] in the middle. The left compartment had mosaic walls and smooth flooring, while the right compartment had black walls and thin-grid flooring. The experiment consisted of three phases: (i) preconditioning, (ii) conditioning, and (iii) postconditioning phase. During the preconditioning phase (pretest trial) (day 1), each mouse was subjected to the middle compartment with free access to all compartments for 10 min. The conditioning phase (days 2 to d4) consisted of six 30-min training sessions that were carried out during morning and afternoon training. CNO [5 mg/kg, i.p. (intraperitoneally)] was always paired with the less preferred compartment in the afternoon. On day 2, mice were treated with saline (10 ml/kg, i.p.) in the morning training session and immediately paired with the preferred compartment with access blocked for 30 min. In the afternoon, mice were treated with CNO and immediately paired with the less preferred compartment for 30 min. The morning and afternoon training sessions were repeated for 3 days in total from days 2 to 4. In the postconditioning phase (test trial, day 5), each mouse was subjected to the middle compartment with free access to the other compartments in the absence of treatments for 10 min.

In the RTPP, mice were subjected to a place preference chamber (as described above) for 20 min. One counterbalanced side of the chamber was assigned as the stimulation side. The light-emitting diode [Thorlabs, M470F3 (470 nm) and M595F2 (595 nm)] was triggered on the basis of the location of the animal using primmax software and controllers. In the photostimulated side of the arena, which was assigned on the basis of the initial preference, mice received a 470-nm stimulation of 20 Hz with 10 mW of power at the fiber tips. For photoinhibition, mice received constant 595 nm with 10 mW of power at the fiber tips. Bilateral stimulation of freely moving animals was achieved using a fiber optic rotary joint (FRJ_1 × 2i_FC-2FC, Doric). Behavioral data were recorded via a charge-coupled device camera.

Gradient index lens implantation and baseplate fixation

The gradient index (GRIN) lens was implanted 1 week after viral injection ($AAV_{2/1}$-hSyn-GCaMP6s) in the SN. Mice were anesthetized as described above. Debris was removed from the hole and a customized blunted 20-gauge needle (1 mm in diameter) was slowly lowered down into the brain (AP: −3, ML: 1.65, DV: −3.95 mm). After retraction of the needle, a GRIN lens (ProView lens; diameter, 0.6 mm; length, ~7.4 mm; Inscopix) mounted on a GRIN lens holder was slowly implanted above the lateral SN. The exposed skull was covered with dental acrylic (Paladur, Heraeus). Two weeks after GRIN lens implantation, mice were anesthetized and placed in the stereotaxic frame. A baseplate (BPL-2, Inscopix) attached to a miniature microscope was positioned above the GRIN lens. The focal plane was adjusted until neuronal structures and GCaMP6s dynamics were observed. The baseplate was fixed using C&B-Metabond (Parkell).

In vivo calcium imaging

For simultaneous recording of GCaMP6s fluorescence signals and light activation of terminals in the SN, a miniature microscope system for integrated calcium imaging and optogenetics was used (nVoke 2.0, Inscopix). Mice were habituated to the miniscope 3 days before the behavioral experiment. The basal level of calcium activity was recorded in the first 5 min after CNO application. Then, the effect of GPe^{CRHR1} neuron activity was measured by illuminating ChrimsonR-expressing terminals in the SN (590 nm, 10 mW, 20 Hz) for 5 min. Another 5 min later, CNO reached its full effect on hM3Dq-expressing $IPACL^{CRH}$ neurons. Thus, the recorded activity of cells in the next 5 min reflected both light-induced activation of GPe^{CRHR1} and CNO-induced activation of $IPACL^{CRH}$ neurons. Cell activities recorded in the last 5 min correspond to CNO-activated $IPACL^{CRH}$ neurons. Image acquisition and behavior were synchronized. For imaging data processing and analysis, we used the Inscopix data processing software (version 1.3.0).

Corticosterone measurement

Plasma corticosterone concentrations were measured as previously described (*9*) using a commercially available radioimmunoassay kit (MP Biomedicals) according to the manufacturer's instructions.

Statistical analysis

No statistical methods were used to predetermine sample sizes. The numbers of samples in each group were based on those in previously published studies. The means ± SEM were determined for each group. Figure generation and statistical calculation were conducted by Graphpad Prism 9 software. Two-tailed Student's *t* test was performed for comparison between two groups with one variation. One-way analysis of variance (ANOVA) was used for one group with multiple variations. Two-way ANOVA was performed for two groups with multiple variations; Bonferroni's post hoc test was used for multiple comparisons. Repeated-measures two-way ANOVA was performed with two groups with continuous variations (time), and Bonferroni's post hoc test was used for multiple comparisons. Differences were considered significant when P was smaller than 0.05.

SUPPLEMENTARY MATERIALS

Supplementary material for this article is available at https://science.org/doi/10.1126/sciadv.abo1023

REFERENCES AND NOTES

1. M. Joëls, T. Z. Baram, The neuro-symphony of stress. *Nat. Rev. Neurosci.* **10**, 459–466 (2009).
2. E. P. Zorrilla, M. L. Logrip, G. F. Koob, Corticotropin releasing factor: A key role in the neurobiology of addiction. *Front. Neuroendocrinol.* **35**, 234–244 (2014).
3. B. S. McEwen, N. P. Bowles, J. D. Gray, M. N. Hill, R. G. Hunter, I. N. Karatsoreos, C. Nasca, Mechanisms of stress in the brain. *Nat. Neurosci.* **18**, 1353–1363 (2015).
4. J. M. Deussing, A. Chen, The corticotropin-releasing factor family: Physiology of the stress response. *Physiol. Rev.* **98**, 2225–2286 (2018).

5. W. Vale, J. Spiess, C. Rivier, J. Rivier, Characterization of a 41-residue ovine hypothalamic peptide that stimulates secretion of corticotropin and β-endorphin. *Science* **213**, 1394–1397 (1981).
6. C. A. Lowry, F. L. Moore, Regulation of behavioral responses by corticotropin-releasing factor. *Gen. Comp. Endocrinol.* **146**, 19–27 (2006).
7. R. E. Sutton, G. F. Koob, M. Le Moal, J. Rivier, W. Vale, Corticotropin releasing factor produces behavioural activation in rats. *Nature* **297**, 331–333 (1982).
8. S. C. Heinrichs, G. F. Koob, Corticotropin-releasing factor in brain: A role in activation, arousal, and affect regulation. *J. Pharmacol. Exp. Ther.* **311**, 427–440 (2004).
9. D. Refojo, M. Schweizer, C. Kuehne, S. Ehrenberg, C. Thoeringer, A. M. Vogl, N. Dedic, M. Schumacher, G. von Wolff, C. Avrabos, C. Touma, D. Engblom, G. Schütz, K.-A. Nave, M. Eder, C. T. Wotjak, I. Sillaber, F. Holsboer, W. Wurst, J. M. Deussing, Glutamatergic and dopaminergic neurons mediate anxiogenic and anxiolytic effects of CRHR1. *Science* **333**, 1903–1907 (2011).
10. T. Füzesi, N. Daviu, J. I. Wamsteeker Cusulin, R. P. Bonin, J. S. Bains, Hypothalamic CRH neurons orchestrate complex behaviours after stress. *Nat. Commun.* **7**, 11937 (2016).
11. J. G. McCall, R. al-Hasani, E. R. Siuda, D. Y. Hong, A. J. Norris, C. P. Ford, M. R. Bruchas, CRH engagement of the locus coeruleus noradrenergic system mediates stress-induced anxiety. *Neuron* **87**, 605–620 (2015).
12. C. A. Sanford, M. E. Soden, M. A. Baird, S. M. Miller, J. Schulkin, R. D. Palmiter, M. Clark, L. S. Zweifel, A central amygdala CRF circuit facilitates learning about weak threats. *Neuron* **93**, 164–178 (2017).
13. N. Dedic, C. Kühne, M. Jakovcevski, J. Hartmann, A. J. Genewsky, K. S. Gomes, E. Anderzhanova, M. L. Pöhlmann, S. Chang, A. Kolarz, A. M. Vogl, J. Dine, M. W. Metzger, B. Schmid, R. C. Almada, K. J. Ressler, C. T. Wotjak, V. Grinevich, A. Chen, M. V. Schmidt, W. Wurst, D. Refojo, J. M. Deussing, Chronic CRH depletion from GABAergic, long-range projection neurons in the extended amygdala reduces dopamine release and increases anxiety. *Nat. Neurosci.* **21**, 803–807 (2018).
14. M. B. Pomrenze, J. Tovar-Diaz, A. Blasio, R. Maiya, S. M. Giovanetti, K. Lei, H. Morikawa, F. W. Hopf, R. O. Messing, A corticotropin releasing factor network in the extended amygdala for anxiety. *J. Neurosci.* **39**, 1030–1043 (2019).
15. M. J. Henckens, J. M. Deussing, A. Chen, Region-specific roles of the corticotropin-releasing factor-urocortin system in stress. *Nat. Rev. Neurosci.* **17**, 636–651 (2016).
16. E. R. de Kloet, M. Joëls, F. Holsboer, Stress and the brain: From adaptation to disease. *Nat. Rev. Neurosci.* **6**, 463–475 (2005).
17. P. D. Butler, J. M. Weiss, J. C. Stout, C. B. Nemeroff, Corticotropin-releasing factor produces fear-enhancing and behavioral activating effects following infusion into the locus coeruleus. *J. Neurosci.* **10**, 176–183 (1990).
18. A. Lu, M. A. Steiner, N. Whittle, A. M. Vogl, S. M. Walser, M. Ableitner, D. Refojo, M. Ekker, J. L. Rubenstein, G. K. Stalla, N. Singewald, F. Holsboer, C. T. Wotjak, W. Wurst, J. M. Deussing, Conditional mouse mutants highlight mechanisms of corticotropin-releasing hormone effects on stress-coping behavior. *Mol. Psychiatry* **13**, 1028–1042 (2008).
19. A. Contarino, F. Dellu, G. F. Koob, G. W. Smith, K. Lee, W. W. Vale, L. H. Gold, Dissociation of locomotor activation and suppression of food intake induced by CRF in CRFR1-deficient mice. *Endocrinology* **141**, 2698–2702 (2000).
20. Y. Chen, J. Molet, B. G. Gunn, K. Ressler, T. Z. Baram, Diversity of reporter expression patterns in transgenic mouse lines targeting corticotropin-releasing hormone-expressing neurons. *Endocrinology* **156**, 4769–4780 (2015).
21. N. Dedic, A. Chen, J. M. Deussing, The CRF family of neuropeptides and their receptors - Mediators of the central stress response. *Curr. Mol. Pharmacol.* **11**, 4–31 (2018).
22. Y. Wang, P. Hu, Q. Shan, C. Huang, Z. Huang, P. Chen, A. Li, H. Gong, J. N. Zhou, Single-cell morphological characterization of CRH neurons throughout the whole mouse brain. *BMC Biol.* **19**, 47 (2021).
23. C. A. Itoga, Y. Chen, C. Fateri, P. A. Echeverry, J. M. Lai, J. Delgado, S. Badhon, A. Short, T. Z. Baram, X. Xu, New viral-genetic mapping uncovers an enrichment of corticotropin-releasing hormone-expressing neuronal inputs to the nucleus accumbens from stress-related brain regions. *J. Comp. Neurol.* **527**, 2474–2487 (2019).
24. J. N. Li, K. Chen, P. L. Sheets, Topographic organization underlies intrinsic and morphological heterogeneity of central amygdala neurons expressing corticotropin-releasing hormone. *J. Comp. Neurol.* **530**, 2286–2303 (2022).
25. C. A. Marcinkiewcz, C. M. Mazzone, G. D'Agostino, L. R. Halladay, J. A. Hardaway, J. F. DiBerto, M. Navarro, N. Burnham, C. Cristiano, C. E. Dorrier, G. J. Tipton, C. Ramakrishnan, T. Kozicz, K. Deisseroth, T. E. Thiele, Z. A. McElligott, A. Holmes, L. K. Heisler, T. L. Kash, Serotonin engages an anxiety and fear-promoting circuit in the extended amygdala. *Nature* **537**, 97–101 (2016).
26. E. A. Kelly, J. L. Fudge, The neuroanatomic complexity of the CRF and DA systems and their interface: What we still don't know. *Neurosci. Biobehav. Rev.* **90**, 247–259 (2018).
27. J. C. Lemos, M. J. Wanat, J. S. Smith, B. A. S. Reyes, N. G. Hollon, E. J. van Bockstaele, C. Chavkin, P. E. M. Phillips, Severe stress switches CRF action in the nucleus accumbens from appetitive to aversive. *Nature* **490**, 402–406 (2012).
28. C. Jiang, X. Yang, G. He, F. Wang, Z. Wang, W. Xu, Y. Mao, L. Ma, F. Wang, CRHCeA→VTA inputs inhibit the positive ensembles to induce negative effect of opiate withdrawal. *Mol. Psychiatry* **26**, 6170–6186 (2021).
29. M. J. Wanat, F. W. Hopf, G. D. Stuber, P. E. Phillips, A. Bonci, Corticotropin-releasing factor increases mouse ventral tegmental area dopamine neuron firing through a protein kinase C-dependent enhancement of Ih. *J. Physiol.* **586**, 2157–2170 (2008).
30. N. G. Hollon, L. M. Burgeno, P. E. Phillips, Stress effects on the neural substrates of motivated behavior. *Nat. Neurosci.* **18**, 1405–1412 (2015).
31. L. T. Coddington, J. T. Dudman, Learning from action: Reconsidering movement signaling in midbrain dopamine neuron activity. *Neuron* **104**, 63–77 (2019).
32. E. H. Douma, E. R. de Kloet, Stress-induced plasticity and functioning of ventral tegmental dopamine neurons. *Neurosci. Biobehav. Rev.* **108**, 48–77 (2020).
33. G. D. Stanwood, in *Stress: Physiology, Biochemistry, and Pathology*, G. Fink, Ed. (Academic Press, 2019), pp. 105–114.
34. S. J. Shammah-Lagnado, G. F. Alheid, L. Heimer, Striatal and central extended amygdala parts of the interstitial nucleus of the posterior limb of the anterior commissure: Evidence from tract-tracing techniques in the rat. *J. Comp. Neurol.* **439**, 104–126 (2001).
35. T. Koos, J. M. Tepper, Inhibitory control of neostriatal projection neurons by GABAergic interneurons. *Nat. Neurosci.* **2**, 467–472 (1999).
36. E. S. Nisenbaum, Z. C. Xu, C. J. Wilson, Contribution of a slowly inactivating potassium current to the transition to firing of neostriatal spiny projection neurons. *J. Neurophysiol.* **71**, 1174–1189 (1994).
37. M. Watabe-Uchida, L. Zhu, S. K. Ogawa, A. Vamanrao, N. Uchida, Whole-brain mapping of direct inputs to midbrain dopamine neurons. *Neuron* **74**, 858–873 (2012).
38. A. J. Hunt Jr., R. Dasgupta, S. Rajamanickam, Z. Jiang, M. Beierlein, C. S. Chan, N. J. Justice, Paraventricular hypothalamic and amygdalar CRF neurons synapse in the external globus pallidus. *Brain Struct. Funct.* **223**, 2685–2698 (2018).
39. D. R. Britton, G. F. Koob, J. Rivier, W. Vale, Intraventricular corticotropin-releasing factor enhances behavioral effects of novelty. *Life Sci.* **31**, 363–367 (1982).
40. K. T. Britton, G. Lee, W. Vale, J. Rivier, G. F. Koob, Corticotropin releasing factor (CRF) receptor antagonist blocks activating and 'anxiogenic' actions of CRF in the rat. *Brain Res.* **369**, 303–306 (1986).
41. A. Tazi, N. R. Swerdlow, M. LeMoal, J. Rivier, W. Vale, G. F. Koob, Behavioral activation by CRF: Evidence for the involvement of the ventral forebrain. *Life Sci.* **41**, 41–49 (1987).
42. P. W. Kalivas, P. Duffy, L. G. Latimer, Neurochemical and behavioral effects of corticotropin-releasing factor in the ventral tegmental area of the rat. *J. Pharmacol. Exp. Ther.* **242**, 757–763 (1987).
43. A. J. Dunn, C. W. Berridge, Is corticotropin-releasing factor a mediator of stress responses? *Ann. N. Y. Acad. Sci.* **579**, 183–191 (1990).
44. M. Cador, S. Dumas, B. J. Cole, J. Mallet, G. F. Koob, M. Le Moal, L. Stinus, Behavioral sensitization induced by psychostimulants or stress: Search for a molecular basis and evidence for a CRF-dependent phenomenon. *Ann. N. Y. Acad. Sci.* **654**, 416–420 (1992).
45. D. H. Tanaka, S. Li, S. Mukae, T. Tanabe, Genetic access to gustatory disgust-associated neurons in the interstitial nucleus of the posterior limb of the anterior commissure in male mice. *Neuroscience* **413**, 45–63 (2019).
46. B. G. Gunn, C. D. Cox, Y. Chen, M. Frotscher, C. M. Gall, T. Z. Baram, G. Lynch, The endogenous stress hormone CRH modulates excitatory transmission and network physiology in Hippocampus. *Cereb. Cortex* **27**, 4182–4198 (2017).
47. J. Liu, B. Yu, V. Neugebauer, D. E. Grigoriadis, J. Rivier, W. W. Vale, P. Shinnick-Gallagher, J. P. Gallagher, Corticotropin-releasing factor and Urocortin I modulate excitatory glutamatergic synaptic transmission. *J. Neurosci.* **24**, 4020–4029 (2004).
48. B. A. Harlan, H. C. Becker, J. J. Woodward, A. C. Riegel, Opposing actions of CRF-R1 and CB1 receptors on VTA-GABAergic plasticity following chronic exposure to ethanol. *Neuropsychopharmacology* **43**, 2064–2074 (2018).
49. Z. Nie, P. Schweitzer, A. J. Roberts, S. G. Madamba, S. D. Moore, G. R. Siggins, Ethanol augments GABAergic transmission in the central amygdala via CRF1 receptors. *Science* **303**, 1512–1514 (2004).
50. C. L. Williams, W. C. Buchta, A. C. Riegel, CRF-R2 and the heterosynaptic regulation of VTA glutamate during reinstatement of cocaine seeking. *J. Neurosci.* **34**, 10402–10414 (2014).
51. D. M. Lovinger, Y. Mateo, K. A. Johnson, S. A. Engi, M. Antonazzo, J. F. Cheer, Local modulation by presynaptic receptors controls neuronal communication and behaviour. *Nat. Rev. Neurosci.* **23**, 191–203 (2022).
52. Q. Cui, A. Pamukcu, S. Cherian, I. Y. M. Chang, B. L. Berceau, H. S. Xenias, M. H. Higgs, S. Rajamanickam, Y. Chen, X. du, Y. Zhang, H. McMorrow, Z. A. Abecassis, S. M. Boca, N. J. Justice, C. J. Wilson, C. S. Chan, Dissociable roles of pallidal neuron subtypes in regulating motor patterns. *J. Neurosci.* **41**, 4036–4059 (2021).
53. R. C. Evans, E. L. Twedell, M. Zhu, J. Ascencio, R. Zhang, Z. M. Khaliq, Functional dissection of basal ganglia inhibitory inputs onto substantia nigra dopaminergic neurons. *Cell Rep.* **32**, 108156 (2020).

54. K. J. Mastro, R. S. Bouchard, H. A. Holt, A. H. Gittis, Transgenic mouse lines subdivide external segment of the globus pallidus (GPe) neurons and reveal distinct GPe output pathways. *J. Neurosci.* **34**, 2087–2099 (2014).
55. J. M. Deniau, P. Mailly, N. Maurice, S. Charpier, The pars reticulata of the substantia nigra: A window to basal ganglia output. *Prog. Brain Res.* **160**, 151–172 (2007).
56. G. Rizzi, K. R. Tan, Synergistic nigral output pathways shape movement. *Cell Rep.* **27**, 2184–2198.e4 (2019).
57. S. Hormigo, G. Vega-Flores, M. A. Castro-Alamancos, Basal ganglia output controls active avoidance behavior. *J. Neurosci.* **36**, 10274–10284 (2016).
58. C. R. Lee, J. M. Tepper, Morphological and physiological properties of parvalbumin- and calretinin-containing γ-aminobutyric acidergic neurons in the substantia nigra. *J. Comp. Neurol.* **500**, 958–972 (2007).
59. E. E. Steinberg, F. Gore, B. D. Heifets, M. D. Taylor, Z. C. Norville, K. T. Beier, C. Földy, T. N. Lerner, L. Luo, K. Deisseroth, R. C. Malenka, Amygdala-midbrain connections modulate appetitive and aversive learning. *Neuron* **106**, 1026–1043.e9 (2020).
60. R. A. Wise, Roles for nigrostriatal—Not just mesocorticolimbic—Dopamine in reward and addiction. *Trends Neurosci.* **32**, 517–524 (2009).
61. H. Taniguchi, M. He, P. Wu, S. Kim, R. Paik, K. Sugino, D. Kvitsani, Y. Fu, J. Lu, Y. Lin, G. Miyoshi, Y. Shima, G. Fishell, S. B. Nelson, Z. J. Huang, A resource of Cre driver lines for genetic targeting of GABAergic neurons in cerebral cortex. *Neuron* **71**, 995–1013 (2011).
62. G. J. Salimando, M. Hyun, K. M. Boyt, D. G. Winder, BNST GluN2D-containing NMDA receptors influence anxiety- and depressive-like behaviors and modulatecell-specific excitatory/inhibitory synaptic balance. *J. Neurosci.* **40**, 3949–3968 (2020).
63. S. Hippenmeyer, E. Vrieseling, M. Sigrist, T. Portmann, C. Laengle, D. R. Ladle, S. Arber, A developmental switch in the response of DRG neurons to ETS transcription factor signaling. *PLoS Biol.* **3**, e159 (2005).
64. J. F. Poulin, G. Caronia, C. Hofer, Q. Cui, B. Helm, C. Ramakrishnan, C. S. Chan, D. A. Dombeck, K. Deisseroth, R. Awatramani, Mapping projections of molecularly defined dopamine neuron subtypes using intersectional genetic approaches. *Nat. Neurosci.* **21**, 1260–1271 (2018).
65. C. Gizowski, C. W. Bourque, Sodium regulates clock time and output via an excitatory GABAergic pathway. *Nature* **583**, 421–424 (2020).
66. A. Mo, E. A. Mukamel, F. P. Davis, C. Luo, G. L. Henry, S. Picard, M. A. Urich, J. R. Nery, T. J. Sejnowski, R. Lister, S. R. Eddy, J. R. Ecker, J. Nathans, Epigenomic signatures of neuronal diversity in the mammalian brain. *Neuron* **86**, 1369–1384 (2015).
67. L. Madisen, T. A. Zwingman, S. M. Sunkin, S. W. Oh, H. A. Zariwala, H. Gu, L. L. Ng, R. D. Palmiter, M. J. Hawrylycz, A. R. Jones, E. S. Lein, H. Zeng, A robust and high-throughput Cre reporting and characterization system for the whole mouse brain. *Nat. Neurosci.* **13**, 133–140 (2010).
68. L. Madisen, A. R. Garner, D. Shimaoka, A. S. Chuong, N. C. Klapoetke, L. Li, A. van der Bourg, Y. Niino, L. Egolf, C. Monetti, H. Gu, M. Mills, A. Cheng, B. Tasic, T. N. Nguyen, S. M. Sunkin, A. Benucci, A. Nagy, A. Miyawaki, F. Helmchen, R. M. Empson, T. Knöpfel, E. S. Boyden, R. C. Reid, M. Carandini, H. Zeng, Transgenic mice for intersectional targeting of neural sensors and effectors with high specificity and performance. *Neuron* **85**, 942–958 (2015).
69. F. A. Wolf, P. Angerer, F. J. Theis, SCANPY: Large-scale single-cell gene expression data analysis. *Genome Biol.* **19**, 15 (2018).
70. A. T. Lun, D. J. McCarthy, J. C. Marioni, A step-by-step workflow for low-level analysis of single-cell RNA-seq data with Bioconductor. *F1000Res.* **5**, 2122 (2016).
71. S. L. Wolock, R. Lopez, A. M. Klein, Scrublet: Computational identification of cell doublets in single-cell transcriptomic data. *Cell Syst.* **8**, 281–291.e9 (2019).
72. E. Z. Macosko, A. Basu, R. Satija, J. Nemesh, K. Shekhar, M. Goldman, I. Tirosh, A. R. Bialas, N. Kamitaki, E. M. Martersteck, J. J. Trombetta, D. A. Weitz, J. R. Sanes, A. K. Shalek, A. Regev, S. A. McCarroll, Highly parallel genome-wide expression profiling of individual cells using nanoliter droplets. *Cell* **161**, 1202–1214 (2015).
73. C. Chen, K. M. Wilcoxen, C. Q. Huang, Y.-F. Xie, J. R. McCarthy, T. R. Webb, Y.-F. Zhu, J. Saunders, X.-J. Liu, T.-K. Chen, H. Bozigian, D. E. Grigoriadis, Design of 2,5-dimethyl-3-(6-dimethyl-4-methylpyridin-3-yl)-7-dipropylaminopyrazolo[1,5-a]pyrimidine (NBI 30775/R121919) and structure--activity relationships of a series of potent and orally active corticotropin-releasing factor receptor antagonists. *J. Med. Chem.* **47**, 4787–4798 (2004).

Acknowledgments: We would like to thank A. Varga, head of the animal facility, and staff for the dedicated support with animal care; S. Unkmeir, S. Bauer, and the scientific core unit Genetically Engineered Mouse Models for genotyping support; E. Fesl and J. Keverne for proofreading and editing of the manuscript. We thank C. Wotjak for input and critical discussion; M. Götz, S. Cappello, and K.-K. Conzelmann for the technical support. **Funding:** This work was funded by Max Planck Society (to J.M.D.); German Ministry of Science and Education, IMADAPT, FKZ 01KU1901 (to J.M.D.); German Research Foundation (project-ID 118803580), SFB 870 Z1 (to A.A.H.); Marie Skłodowska-Curie innovative training network PurinesDX, grant agreement ID: 766124 (to J.M.D.); and European Research Council (ERC), Redesigning brain circuits in development, BrainRedesign, grant agreement ID: 885192 (to R.K.). **Author contributions:** Conceptualization: S.C. and J.M.D. Methodology: F.F., C.-L.L., A.A.H., and R.K. Investigation: S.C., F.F., C.-L.L., L.H., M.J., R.D.G., M.G., D.M., and J.M.D. Data analysis: S.C., L.H., R.D.G., M.Z., M.E., N.C., and J.M.D. Visualization: S.C., L.H., R.D.G., M.E., and J.M.D. Funding acquisition: J.M.D. Project administration: J.M.D. Supervision: M.Z., M.E., N.C., and J.M.D. Writing (original draft): J.M.D. and S.C. Writing (review and editing): S.C., M.J., M.E., N.C., and J.M.D. **Competing interests:** The authors declare that they have no competing interests. **Data and materials availability:** All data needed to evaluate the conclusions in the paper are present in the paper and/or the Supplementary Materials. Mouse lines CRHR1-Cre, $CRHR1^{\Delta\text{-}EGFP}$, and $CRHR1^{N\text{-}EGFP}$ are available from J.M.D. under a material agreement with the Max Planck Institute of Psychiatry.

Submitted 13 January 2022
Accepted 30 September 2022
Published 16 November 2022
10.1126/sciadv.abo1023